

# Creating geometrically robust designs for highly sensitive problems using topology optimization

## Acoustic cavity design

Rasmus E. Christiansen<sup>1</sup> · Boyan S. Lazarov<sup>1</sup> · Jakob S. Jensen<sup>2</sup> · Ole Sigmund<sup>1</sup>

Received: 26 August 2014 / Revised: 7 April 2015 / Accepted: 7 May 2015 / Published online: 21 June 2015  
© Springer-Verlag Berlin Heidelberg 2015

**Abstract** Resonance and wave-propagation problems are known to be highly sensitive towards parameter variations. This paper discusses topology optimization formulations for creating designs that perform robustly under spatial variations for acoustic cavity problems. For several structural problems, robust topology optimization methods have already proven their worth. However, it is shown that direct application of such methods is not suitable for the acoustic problem under consideration. A new double filter approach is suggested which makes robust optimization for spatial variations possible. Its effect and limitations are discussed. In addition, a known explicit penalization approach is considered for comparison. For near-uniform spatial variations it is shown that highly robust designs can be obtained using the double filter approach. It is finally demonstrated that taking non-uniform variations into account further improves the robustness of the designs.

**Keywords** Topology optimization · Robust design · Wave propagation · Acoustics · Noise reduction · Projection filtering · Uniform design variations · Non-uniform design variations

## 1 Introduction

It is widely known that solutions to interior acoustic problems in the medium to high frequency range are highly sensitive to parameter variations (Jacobsen and Juhl 2013). For high frequencies the problems are so sensitive that only statistical methods are viable, e.g. statistical energy analysis (Lyon and DeJONG 1998). In this paper we are interested in deterministic solutions for the pressure field and thus restrict ourselves to the low/medium frequency range. We consider a 2D interior acoustics problem with reflecting boundaries for single frequencies. We seek to minimize the sound pressure in part of the domain utilizing interference phenomena by placing material in the domain using topology optimization (Bendsøe and Sigmund 2003). We base our approach on the work by Dühring et al. (2008) where the topology optimization formulation for interior acoustic problems was presented. It was shown to be possible to significantly reduce the sound pressure in a designated part of the domain by placing material elsewhere. We demonstrate that the pressure field is very sensitive to variations in the geometry of the optimized design even at medium frequencies. This is problematic from an application point of view since it is likely impossible to manufacture or install the designs exactly to specifications, leaving the designs useless in real world applications.

We present a topology optimization based approach for creating designs that maintain high performance under substantial near-uniform and small non-uniform geometric variations. For problems in structural mechanics, heat conduction (Wang et al. 2011b), and optics (Wang et al. 2011a; Elesin et al. 2012), it has been shown that using a robust optimization approach leads to a significant improvement in the robustness of the design's performance under spatial variations. We base our approach on the work by

---

✉ Rasmus E. Christiansen  
raelch@mek.dtu.dk

<sup>1</sup> Department of Mechanical Engineering, Solid Mechanics, Technical University of Denmark, Nils Koppels Alle, B. 404, 2800 Lyngby, Denmark

<sup>2</sup> Department of Electrical Engineering, Centre for Acoustic-Mechanical Micro Systems, Technical University of Denmark, Ørstedes Plads, B. 352, 2800 Lyngby, Denmark

Wang et al. (2011b). Here the design is optimized for a nominal, an eroded and a dilated realization simultaneously using a min/max formulation. The realizations are obtained using continuous projection of smoothed design variables. We demonstrate that applying the robust scheme directly is insufficient for the present acoustic problem due to unpredictable variations in the eroded and dilated designs, making it impossible to perform meaningful robust optimization. To alleviate the problem we present a double filter which restricts design features to vary along their edges as the projection level changes. This allows for optimization of designs towards geometric variations. Promising results for designs optimized under both near-uniform and non-uniform geometric variations are presented. A related double filter approach developed independently of the approach presented in this paper is used in a structural mechanics topology optimization formulation for creating coated structures (Clausen et al. 2015). Other papers have treated and demonstrated the usefulness of topology optimization for problems in acoustics e.g. Wadbro and Berggren (2006), Lee and Kim (2009), Kook et al. (2012), and Wadbro (2014) and for acoustic structure interaction, e.g. Yoon et al. (2007) and Du and Olhoff (2007). The question of geometric robustness of the designs have, to our knowledge, not been investigated elsewhere. As a final note it is stressed that the optimization problems considered here are highly non-convex. Hence small changes in problem or optimization parameters may lead the optimization procedure to converge to different robust designs.

## 2 Model problem

We seek to minimize the square of the average sound pressure amplitude,  $|\hat{p}|^2$ , in the sub-domain  $\Omega_{OP}$  of the model domain  $\Omega \subset \mathbb{R}^2$ . A small source domain  $\mathbf{P}$  is used to excite acoustic waves. The reduction in  $|\hat{p}|^2$  is achieved by introducing solid material in a region  $\Omega_d$  replacing the acoustic medium.  $\Omega_{OP}$ ,  $\Omega_d$  and  $\mathbf{P}$  are sub-domains of  $\Omega$  and are assumed to be non-intersecting. The boundary of  $\Omega$ , denoted  $\delta\Omega$ , is taken to be perfectly reflecting. Figure 1 shows the domain configuration used, unless otherwise noted.

## 3 Physics model

Time-harmonic acoustic wave-propagation in an adiabatic medium is governed by the Helmholtz equation,

$$\nabla \cdot (\rho(\mathbf{x})^{-1} \nabla \hat{p}(\mathbf{x})) + \omega^2 \kappa(\mathbf{x})^{-1} \hat{p}(\mathbf{x}) = 0, \quad \mathbf{x} \in \Omega. \quad (1)$$

Here  $\nabla$  denotes the spatial derivative,  $\hat{p}$  is the complex sound pressure and  $\rho$  and  $\kappa$  are the density and bulk

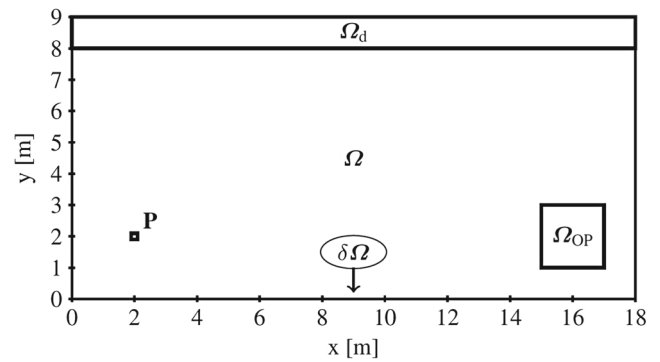


**Fig. 1** Illustration of the domain configuration,  $\Omega = [0, 18] \times [0, 9]$ ,  $\Omega_{OP} = [15, 17] \times [1, 3]$  is the optimization domain,  $\Omega_d = [0, 18] \times [8, 9]$  is the design domain and  $\mathbf{P} = [1.9, 2.1] \times [1.9, 2.1]$  denotes the region where an acoustic wave is exited

modulus of the medium, respectively.  $\omega = 2\pi f$  is the angular frequency where  $f$  is denoted the excitation frequency. The spatial dependence in (1) is suppressed in the following for brevity. The perfectly reflecting boundaries and the source are imposed using,

$$\mathbf{n} \cdot (\rho^{-1} \nabla \hat{p}) = 0, \quad \forall \mathbf{x} \in \delta\Omega, \quad (2)$$

$$\mathbf{n} \cdot (\rho^{-1} \nabla \hat{p}) = -i\omega U, \quad \forall \mathbf{x} \in \delta\mathbf{P}. \quad (3)$$

Here  $\mathbf{n}$  is the outward pointing normal vector to the boundary in question and  $U$  is the vibrational velocity.

The material parameters of solid and air are chosen to have a very large contrast between them. This justifies disregarding the structural problem of the solid material as it will simply act as hard wall boundary conditions for the acoustic waves. The material parameters have been chosen to match those for atmospheric air and aluminum given by,

$$\text{air: } \rho_1 = 1.204 \text{ kg m}^{-3}, \quad \kappa_1 = 141.921 \cdot 10^3 \text{ N m}^{-2}. \quad (4)$$

$$\text{Al: } \rho_2 = 2643.0 \text{ kg m}^{-3}, \quad \kappa_2 = 6.87 \cdot 10^{10} \text{ N m}^{-2}. \quad (5)$$

We perform a rescaling of the parameters in the model,

$$(\hat{\rho}, \hat{\kappa}) = \begin{cases} (1, 1) & \text{air} \\ \left(\frac{\rho_2}{\rho_1}, \frac{\kappa_2}{\kappa_1}\right) & \text{solid} \end{cases}, \quad \hat{\omega} = \frac{\omega}{c}, \quad c = \sqrt{\frac{\kappa_1}{\rho_1}}, \quad (6)$$

where  $c$  is the speed of sound in the gas (acoustic medium). By applying the rescaling (1), (2) and (3) becomes,

$$\nabla \cdot (\hat{\rho}^{-1} \nabla \hat{p}) + \hat{\omega}^2 \hat{\kappa}^{-1} \hat{p} = 0, \quad \mathbf{x} \in \Omega, \quad (7)$$

$$\mathbf{n} \cdot (\hat{\rho}^{-1} \nabla \hat{p}) = 0, \quad \forall \mathbf{x} \in \delta\Omega, \quad (8)$$

$$\mathbf{n} \cdot (\hat{\rho}^{-1} \nabla \hat{p}) = -i\hat{\omega} U \sqrt{\kappa_1 \rho_1}, \quad \forall \mathbf{x} \in \delta\mathbf{P}. \quad (9)$$

All results are reported using the sound pressure level, abbreviated SPL, for a given,  $\hat{p}$ , which is calculated as,

$$L_{\hat{p}} = 10 \log_{10} \left( \frac{|\hat{p}|^2}{p_{\text{ref}}^2} \right), \quad p_{\text{ref,air}} = 20 \mu\text{Pa}. \quad (10)$$

$p_{\text{ref}}$  is the material dependent reference pressure for air, (Jacobsen and Juhl 2013).

### 4 The optimization problem

Minimizing the average of  $|\hat{p}|^2$  over  $\Omega_{OP}$ , is equivalent to minimizing the average of  $L_{\hat{p}}$  over  $\Omega_{OP}$ , henceforth denoted  $\langle L_{\hat{p}} \rangle_{\Omega_{OP}}$ . The discrete problem of placing material in  $\Omega_d$  is replaced by a continuous problem, see Dühring et al. (2008). A design variable field,  $0 \leq \xi(\mathbf{x}) \leq 1, \forall \mathbf{x} \in \Omega_d, \xi(\mathbf{x}) = 0 \forall \mathbf{x} \in \Omega \setminus \Omega_d$ , is introduced and a linear interpolation of the inverse density and bulk modulus is used. This interpolation is given by,

$$\hat{\rho}(\xi)^{-1} = 1 + \xi \left( \left( \frac{\rho_2}{\rho_1} \right)^{-1} - 1 \right), \tag{11}$$

$$\hat{k}(\xi)^{-1} = 1 + \xi \left( \left( \frac{\kappa_2}{\kappa_1} \right)^{-1} - 1 \right). \tag{12}$$

The optimization problem may be stated as,

$$\begin{aligned} \min_{\xi} : & \Phi = \frac{1}{A_{OP}} \int |\hat{p}(\xi)|^2 d\Omega_{OP}, \quad A_{OP} = \int d\Omega_{OP}, \\ \text{s.t.} : & 0 \leq \xi(\mathbf{x}) \leq 1 \quad \forall \mathbf{x} \in \Omega_d, \end{aligned} \tag{13}$$

Here  $\Phi$  denotes the objective.  $\hat{p}(\xi)$  is obtained by solving (7)–(9) for a given design variable field,  $\xi(\mathbf{x})$ . Solving (13) using the approach outlined in Sections 4–6 is in the rest of the paper denoted as *the standard approach*.

### 5 The discrete problem

The domain  $\Omega$ , governing PDE (7) and corresponding boundary conditions (8)–(9) are discretized using the finite element method (FEM). For the discretization Q4 elements of equal size are used throughout  $\Omega$  with a total of  $\mathcal{N}$  nodes in the mesh. The linear basis function connected to node  $k$  is denoted  $N_k$ . The discretization yields the linear system,

$$\mathbf{S}\hat{\mathbf{p}} = (\mathbf{K}(\hat{\rho}) - \hat{\omega}^2\mathbf{M}(\hat{k}))\hat{\mathbf{p}} = \mathbf{F}. \tag{14}$$

$\mathbf{F}$  stems from the boundary condition (9), and is given as,

$$F_k = \sum_{i \in \mathcal{N}_{b,k}} \int_{\delta\Omega_i} \mathbf{n} \cdot (\hat{\rho}^{-1} \nabla \hat{p}) N_k d\Omega \tag{15}$$

Here  $\mathcal{N}_{b,k}$  denotes the boundary edges connected to node  $k$ .  $\mathbf{K}$  and  $\mathbf{M}$  in (14) are given by,

$$K_{ij} = \int \hat{\rho}^{-1} \nabla N_i \nabla N_j d\Omega, \quad M_{ij} = \int \hat{k}^{-1} N_i N_j d\Omega, \tag{16}$$

where  $i \in \{1, 2, \dots, \mathcal{N}\}, j \in \{1, 2, \dots, \mathcal{N}\}$ . Neither  $\mathbf{M}$  nor  $\mathbf{K}$  needs modifications to take the boundary conditions into account. The solution to (7),  $\hat{p}$ , is approximated by,

$$\hat{p} \approx \sum_{k \in \mathcal{N}} \hat{p}_k N_k, \tag{17}$$

where  $\hat{p}_k$  is the  $k$ 'th entry in  $\hat{\mathbf{p}}$ , the solution of (14).

The design variable field,  $\xi(\mathbf{x})$ , is discretized in a discontinuous manner using piecewise constant values in each finite element.

### 5.1 Sensitivities

The sensitivities required for the topology optimization procedure are obtained using adjoint sensitivity analysis, see Dühring et al. (2008) and references therein. They are,

$$\frac{d\Phi}{d\xi_i} = \frac{\partial \Phi}{\partial \xi_i} + \Re \left( \boldsymbol{\lambda}^T \frac{\partial \mathbf{S}}{\partial \xi_i} \hat{\mathbf{p}} \right). \tag{18}$$

Here  $\Re$  denotes the real part,  $T$  denotes the transpose and  $\boldsymbol{\lambda}$  is obtained by solving,

$$\mathbf{S}^T \boldsymbol{\lambda} = - \left( \frac{\partial \Phi}{\partial \hat{\mathbf{p}}_R} - i \frac{\partial \Phi}{\partial \hat{\mathbf{p}}_I} \right)^T, \quad \hat{\mathbf{p}} = \hat{\mathbf{p}}_R + i \hat{\mathbf{p}}_I, \tag{19}$$

with the  $k$ 'th entry in the right hand side given as,

$$\left( \frac{\partial \Phi}{\partial \hat{\mathbf{p}}_R} - i \frac{\partial \Phi}{\partial \hat{\mathbf{p}}_I} \right)_k = \frac{1}{A_{OP}} \int 2(\hat{p}_R - i \hat{p}_I) N_k d\Omega_{OP}. \tag{20}$$

### 6 Filtering and projection strategy

A density filter is used for smoothing followed by a projection to ensure a 0/1-design, (Guest et al. 2004; Xu et al. 2010; Wang et al. 2011b). In the following  $\tilde{\cdot}$  is used to denote smoothed variables and  $\bar{\cdot}$  denotes projected variables. When multiple operations are applied to a variable the symbols are ordered with the latest operation on top. Equation (21) presents the discretized version of the applied density filter (Bourdin 2001; Bruns and Tortorelli 2001),

$$\tilde{\xi}_i = \frac{\sum_{j \in \mathcal{B}_{e,i}} w(\mathbf{x}_i - \mathbf{x}_j) A_j \xi_j}{\sum_{j \in \mathcal{B}_{e,i}} w(\mathbf{x}_i - \mathbf{x}_j) A_j}. \tag{21}$$

$A_j$  is the area of the  $j$ 'th element,  $\mathcal{B}_{e,i}$  denotes the design variables which are within a given filter radius  $R$  of design variable  $i$ . Here  $\mathbf{x}_j$  is taken to be the average of the nodal positions in element  $j$ . The filter function  $w$  is given by,

$$w(\mathbf{x}) = \begin{cases} R - |\mathbf{x}| & \forall |\mathbf{x}| \leq R \wedge \mathbf{x} \in \Omega_d \\ 0 & \text{otherwise} \end{cases}, \tag{22}$$

where  $R$  is the aforementioned filter radius. To allow the design to vary with projection level along the edge of  $\Omega_d$  facing into the domain an extended filter area reaching outside of  $\Omega_d$  was used. In the extended filter area the design variables are all identically zero. A dashed line is included on all designs presented in figures to denote the edge of  $\Omega_d$ .

The projection operator used is the one suggested by Wang et al. (2011b) and is given as,

$$\bar{\xi}_i = \frac{\tanh(\beta\eta) + \tanh(\beta(\xi_i - \eta))}{\tanh(\beta\eta) + \tanh(\beta(1 - \eta))}, \tag{23}$$

where  $\beta$  is a parameter used to control the sharpness of the projection and  $\eta \in [\xi_{\min}, \xi_{\max}]$  defines the projection level.  $\eta = 0.5$  has been used as the target for the final (nominal) designs in all cases. When applying the density filter and projection the pressure field will depend explicitly on the filtered and projected variables,  $\bar{\xi}$ . Hence the optimization problem (13) and the sensitivities should be modified accordingly.

### 6.1 Modification of sensitivities

Applying the smoothing (21) and projection (23) operations on  $\xi$  requires the following sensitivity modifications,

$$\frac{d\Phi}{d\xi_i} = \sum_{h \in \mathcal{B}_{e,i}} \frac{\partial \bar{\xi}_h}{\partial \xi_i} \frac{\partial \bar{\xi}_h}{\partial \xi_h} \frac{d\Phi}{d\bar{\xi}_h}, \tag{24}$$

with,

$$\frac{\partial \bar{\xi}_h}{\partial \xi_i} = \frac{w(\mathbf{x}_h - \mathbf{x}_i) A_i}{\sum_{j \in N_{e,h}} w(\mathbf{x}_h - \mathbf{x}_j) A_j}, \tag{25}$$

$$\frac{\partial \bar{\xi}_h}{\partial \xi_h} = \frac{\beta \operatorname{sech}^2(\beta(\bar{\xi}_h(\mathbf{x}) - \eta))}{\tanh(\beta\eta) + \tanh(\beta(1 - \eta))}, \tag{26}$$

and  $\frac{d\Phi}{d\bar{\xi}_h}$  given by (18).

### 6.2 $\beta$ -continuation scheme

The projection step is used together with a continuation scheme for  $\beta$ , see Guest et al. (2004), which gradually increases the projection strength during the optimization process. This scheme prevents that the optimization gets stuck prematurely in a local minimum during the first iterations due to the design being projected to 0/1 immediately. A more conservative scheme than the one suggested by Wang et al. (2011b) is used here, see algorithm 1. In the present scheme  $\beta$  is only increased if  $\Phi$  has not changed significantly for  $n_{sc}$  iterations.

---

#### Algorithm 1 $\beta$ continuation scheme

---

- 1: Current objective:  $\Phi_c$ , Previous  $n_{sc}$  objectives:  $\Phi_{n_{sc}}$ .
  - 2: **if** ( $n_{sc}$  or more iterations have occurred since last  $\beta$  increase.) **then**
  - 3:     **if**  $|\Phi_c - \max(\Phi_{n_{sc}})| < \alpha |\Phi_c|$  **then**
  - 4:          $\beta = 1.2 \cdot \beta$ .
  - 5:     **end if**
  - 6: **end if**
  - 7: **return**  $\beta$
- 

## 7 Implementation, validation and parameter choices

MATLAB was used for the implementation and the minimization problems were solved using the Method of Moving Asymptotes, MMA (Svanberg 1987). The MATLAB solver was validated using the method of manufactured solutions and through comparison with COMSOL MULTIPHYSICS Version 4.3b’s acoustics module. COMSOL was also used to validate the performance of selected final designs.

Table 1 lists the parameter values which have been used in all numerical experiments unless stated otherwise.

## 8 Sample solution

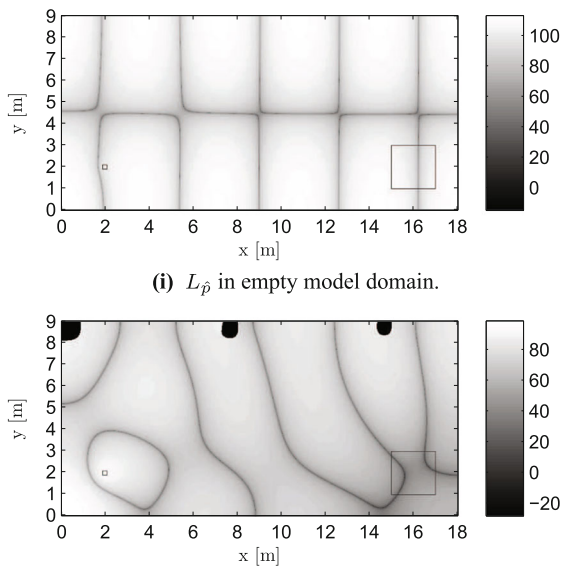
An example of the effect on the pressure field of placing an optimized design in  $\Omega_d$  is presented here. Figure 2i shows the  $L_{\hat{p}}$ -field for the excitation frequency  $f = 51.32$  Hz in an empty domain. Figure 2ii shows the  $L_{\hat{p}}$ -field in the same domain after a design optimized for this frequency using the standard approach is introduced. It is clearly seen that the minimization of  $L_{\hat{p}}$  in  $\Omega_{OP}$  is achieved by a combination of two mechanisms. First a reduction of the overall sound pressure in  $\Omega$  from a maximum of 112 dB to 95 dB has occurred and secondly nodal lines have been moved into  $\Omega_{OP}$  leading to a significant reduction of the average sound pressure level in  $\Omega_{OP}$ ,  $\langle L_{\hat{p}} \rangle_{\Omega_{OP}}$ .

$\langle L_{\hat{p}} \rangle_{\Omega_{OP}}$ , has been reduced from approximately 103 dB for the empty domain to approximately 38.8 dB when the

**Table 1** Parameters used in simulations

Parameter [Unit]	Value
$\mathcal{N}_x$ [elements]	720
$\mathcal{N}_y$ [elements]	360
$\xi_{ini} \forall \mathbf{x} \in \Omega_d$	0.15
$R$ [elements]	20
$U$ [ $\frac{m}{s}$ ]	0.01
$\beta_{init}$	1
$\beta_{max}$	500
$n_{sc}$	10
$\alpha$	0.01
$x_{\Omega} [m] \times y_{\Omega} [m]$	$[0, 18] \times [0, 9]$
$x_{\Omega_d} [m] \times y_{\Omega_d} [m]$	$[0, 18] \times [8, 9]$
$x_{\Omega_{OP}} [m] \times y_{\Omega_{OP}} [m]$	$[15, 17] \times [1, 3]$
$x_{\mathcal{P}} [m] \times y_{\mathcal{P}} [m]$	$[1.9, 2.1] \times [1.9, 2.1]$

$\mathcal{N}_x, \mathcal{N}_y$ : number of elements in the  $x$ - and  $y$ - direction.  $\xi_{ini}$ : initial design variable value.  $R$ : filter radius.  $U$ : vibrational velocity.  $\beta_{ini}, \beta_{max}$ : initial and final  $\beta$ -value.  $n_{sc}$ : minimum iterations between  $\beta$  increases.  $\alpha$ : objective variation parameter.  $x_{\bullet}, y_{\bullet}$ : spatial extend of the domain  $\bullet$



(ii)  $L_{\hat{p}}$  in model domain where optimized design has been introduced.

**Fig. 2** Pressure fields measured using  $L_{\hat{p}}$  at the excitation frequency  $f = 51.32$  Hz. The acoustic source and  $\Omega_{OP}$  are outlined using thin black lines

optimized design is introduced. An important note here is that the magnitude of the reduction in  $\langle L_{\hat{p}} \rangle_{\Omega_{OP}}$  clearly depends on how the nodal lines of the field in the empty room line up with  $\Omega_{OP}$ . In the present example a larger magnitude of the reduction could possibly have been obtained by moving  $\Omega_{OP}$  to  $[13.5, 15.5] \times [1.3]$ . The magnitude of the reduction is not the main interest of this study however. The fact that a significant reduction in sound pressure may be obtained by introducing the design is of course important. It is however the robustness of this reduction towards variations in the design which is the concern in the following.

### 9 Intermediate design variables

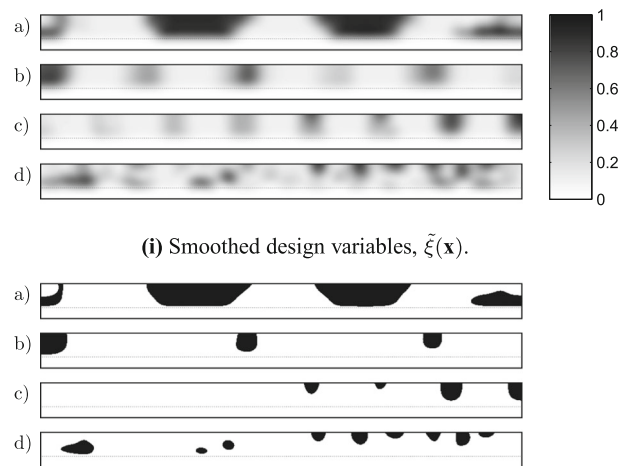
In order for the final designs to be meaningful for real world application they must consist of design variables taking the values 0 or 1, corresponding to no material or material at each position in space. The projection operator presented in (23) enforces a 0/1 design by projecting at the threshold value  $\eta \in [\eta_{min}, \eta_{max}]$ ,  $\eta_{min} \in [0, \eta_{max}[$ ,  $\eta_{max} \in ]\eta_{max}, 1]$ . As described in the introduction it is possible to use a varying projection level,  $\eta$ , to optimize the design towards worst case spatial variations. However, as will be shown in the following there is no guarantee that this approach results in an appropriately varying design. In this context appropriately should be understood as follows: Firstly, when  $\eta$  is varied all changes in the design features should only occur along their edges. Secondly, all design features should change near-uniformly in size if  $\eta$  is varied.

In this section it is shown that for the interior acoustic problem the design does not vary appropriately with  $\eta$  and that this behavior increases significantly with frequency. The issue has been found to exist independent of discretization level and filter radius. Section 9.1 presents the results of solving (13) for four excitation frequencies using the standard approach. In Section 9.2 a min/max formulation for the optimization problem is introduced which will serve as the basis for creating designs that perform robustly under geometric variations. The problem of the inappropriately varying designs is shown to exist for both approaches.

### 9.1 Optimizing using the standard approach

An initial attempt at obtaining highly performing designs is made by solving (13) using filtering, (21) and projection (23). Results for four excitation frequencies,  $f \in \{34.36 \text{ Hz}, 51.32 \text{ Hz}, 69.42 \text{ Hz}, 206.3 \text{ Hz}\}$  are presented below. These frequencies have been chosen to coincide with resonances in the empty domain.

The smoothed design variables for the final designs are shown in Fig. 3i while the final designs after projection at  $\eta = 0.5$  are shown in Fig. 3ii. The value for the objective measured in SPL,  $\langle L_{\hat{p}} \rangle_{\Omega_{OP,XX}}$  with an empty design domain **ED**, a full design domain **FD** ( $\xi_i = 1 \forall i$ ), and with the optimized designs introduced **OD**, are shown in Table 2.  $\langle L_{\hat{p}} \rangle_{\Omega_{OP,FD}}$  is included to illustrate the benefit of creating an optimized solution compared to simply attempting to move away from the resonance by filling the design domain with material.



(ii) Final designs. (Physical design variables,  $\tilde{\xi}(x)$  projected at  $\eta = 0.5$ ).

**Fig. 3** (i) Smoothed,  $\tilde{\xi}$ , and (ii) physical,  $\tilde{\xi}$ , design variables for four excitation frequencies, **a)**  $f = 34.36$  Hz, **b)**  $f = 51.32$  Hz, **c)**  $f = 69.42$  Hz, **d)**  $f = 206.3$  Hz. The standard approach has been used for the optimization. The dashed line denote the edge of  $\Omega_d$

**Table 2** Average sound pressure level in  $\Omega_{OP}$  at four different excitation frequencies, for the cases: Empty design domain,  $\langle L_{\hat{\rho}} \rangle_{\Omega_{OPED}}$ . Design domain filled with material;  $\langle L_{\hat{\rho}} \rangle_{\Omega_{OPFD}}$ . Optimized design introduced,  $\langle L_{\hat{\rho}} \rangle_{\Omega_{OPOD}}$

$f$ [Hz]	$\langle L_{\hat{\rho}} \rangle_{\Omega_{OPED}}$ [dB]	$\langle L_{\hat{\rho}} \rangle_{\Omega_{OPFD}}$ [dB]	$\langle L_{\hat{\rho}} \rangle_{\Omega_{OPOD}}$ [dB]
34.36	≈ 114	≈ 80.5	≈ 64.4
51.32	≈ 99.0	≈ 59.0	≈ 38.8
69.42	≈ 127	≈ 91.8	≈ 46.1
206.3	≈ 120	≈ 116	≈ 64.4

A significant reduction in sound pressure level from both  $\langle L_{\hat{\rho}} \rangle_{\Omega_{OPED}}$  and  $\langle L_{\hat{\rho}} \rangle_{\Omega_{OPFD}}$  to  $\langle L_{\hat{\rho}} \rangle_{\Omega_{OPOD}}$  is observed for all cases. By comparing  $\langle L_{\hat{\rho}} \rangle_{\Omega_{OPOD}}$  to  $\langle L_{\hat{\rho}} \rangle_{\Omega_{OPFD}}$  it is seen to be clearly beneficial to create an optimized design. However if the performance of the designs is highly sensitive to small spatial variations they lose much of their attractiveness. Hence it is important to be able to investigate the design’s sensitivity to spatial variations. Considering the smoothed design variables in Fig. 3i large areas of  $\tilde{\xi}(\mathbf{x})$  taking intermediate values can be seen. These intermediate values make it impossible to establish a meaningful relation between the projection level and the resulting variations in the design. Figure 4 shows the smoothed design variables projected at four  $\eta$ -values to clarify this point. It is seen that the changes in the designs lack any uniformity in space and that the topology changes in several cases as  $\eta$  is varied. Thus the formulation needs a modification to remove the problem if varying  $\eta$  is to be a useful measure of robustness of  $\langle L_{\hat{\rho}} \rangle_{\Omega_{OP}}$  towards geometric variations.

**9.2 Robust design**

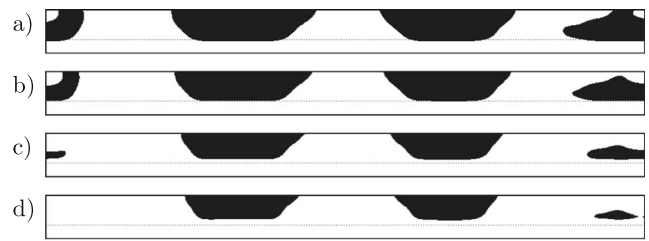
Next we introduce a min/max formulation where the objective is minimized for  $\mathcal{N}_r \in \mathbb{N}$  different realizations of the projected design variables simultaneously<sup>1</sup>.

$$\min_{\xi} : \max_k \left( \frac{1}{A_{OP}} \int |\hat{\rho}(\tilde{\xi}_k)|^2 d\Omega_{OP} \right),$$

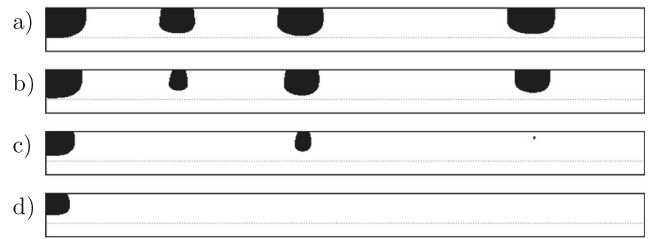
$$\text{s.t.} : 0 \leq \xi(\mathbf{x}) \leq 1 \quad \forall \mathbf{x} \in \Omega_d \wedge k \in \{1, 2, \dots, \mathcal{N}_r\}. \quad (27)$$

Here  $\mathcal{N}_r$  is the number of projection realizations used. In the rest of the paper solving (27) instead of (13) is denoted as *the robust approach*. The min/max formulation forms the basis for creating designs which perform robustly under spatial variations presented in a later section. Direct application of the scheme, suggested for performing robust topology optimization in Sigmund (2009), has been shown to perform

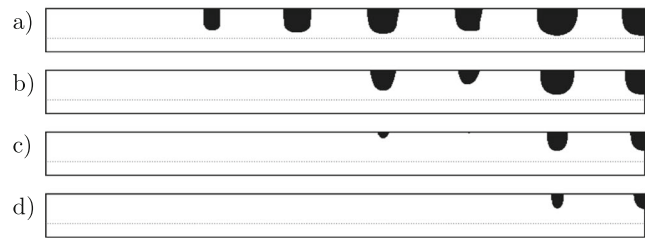
<sup>1</sup>The projection level for each realization may be taken to be constant throughout  $\Omega_d$  or one may introduce a projection-field  $\eta(\mathbf{x})$  which is allowed to vary throughout  $\Omega_d$ , as will be considered in Section 11.



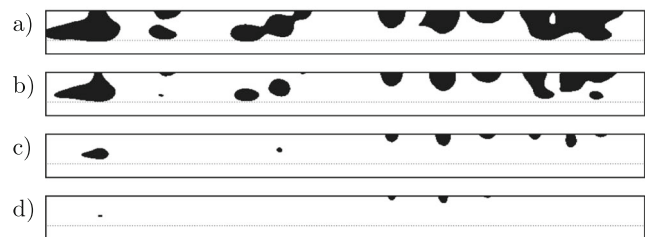
(i) Excitation frequency,  $f = 34.36$  Hz.



(ii) Excitation frequency,  $f = 51.32$  Hz.



(iii) Excitation frequency,  $f = 69.42$  Hz.



(iv) Excitation frequency,  $f = 206.3$  Hz.

**Fig. 4** Projection of smoothed design variables for the four cases shown in Fig. 3 at four  $\eta$ -values, **a)**  $\eta = 0.3$ , **b)**  $\eta = 0.4$ : **c)**  $\eta = 0.6$ , **d)**  $\eta = 0.7$

well for structural and heat problems Wang et al. (2011b) and problems in optics Wang et al. (2011a) when creating robust designs. As will be shown in the following this is not the case for the acoustic cavity problem under consideration.

**9.3 Optimization using the robust approach**

By solving (27), with  $\mathcal{N}_r = 3$  using  $\eta_k \in \{0.3, 0.5, 0.7\}$  new optimized designs have been found for the same four

excitation frequencies.  $\eta_k = 0.5$  corresponds to the desired nominal design while  $\eta_k = 0.3$  and  $\eta_k = 0.7$  corresponds to dilated and eroded versions of the nominal design respectively. The smoothed design variables and the final designs projected at  $\eta = 0.5$  are presented in Fig. 5i and ii respectively. Figure 5i shows that the problem of large areas of non-systematically varying  $\tilde{\xi}(\mathbf{x})$ -values remains for the robust formulation. Again the problem is seen to increase significantly with frequency. The reason why the problem remains when using the robust approach is believed to be the increasing non-convexity of the optimization problem with increasing frequency, caused by the increasing modal density. This leads to a high number of local minima which allows the optimizer to shape the design field such that a variation in  $\eta$  may result in unpredictable variations in the design while still providing good performance for the projected designs at the  $\eta$ -values used in the optimization.

Results of projecting the smoothed design variables presented in Fig. 5i at different  $\eta$ -values are shown in Fig. 6. The results for the design optimized for  $f = 34.36$  Hz seen in Fig. 6 show that using  $\mathcal{N}_r = 3$  instead of a single realization appears to have mitigated the problem of the unpredictable variations in the final design as  $\eta$  is varied. However, the figure clearly illustrates that for  $f \geq 51.32$  Hz the problem of unpredictably varying designs with projection level remains. By comparing Figs. 5ii and 3ii it is seen that the designs for the lowest frequency  $f = 34.36$  Hz are very similar indicating that this design is robust towards variations in its geometry.

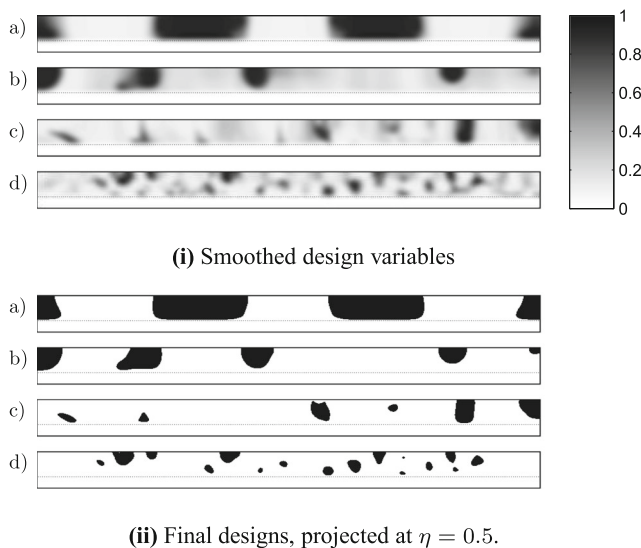


**Fig. 5** (i) Smoothed and (ii) projected design variables for the four excitation frequencies, **a)**  $f = 34.36$  Hz, **b)**  $f = 51.32$  Hz, **c)**  $f = 69.42$  Hz, **d)**  $f = 206.3$  Hz, obtained using the robust approach given in (27) with a smoothing and projection step

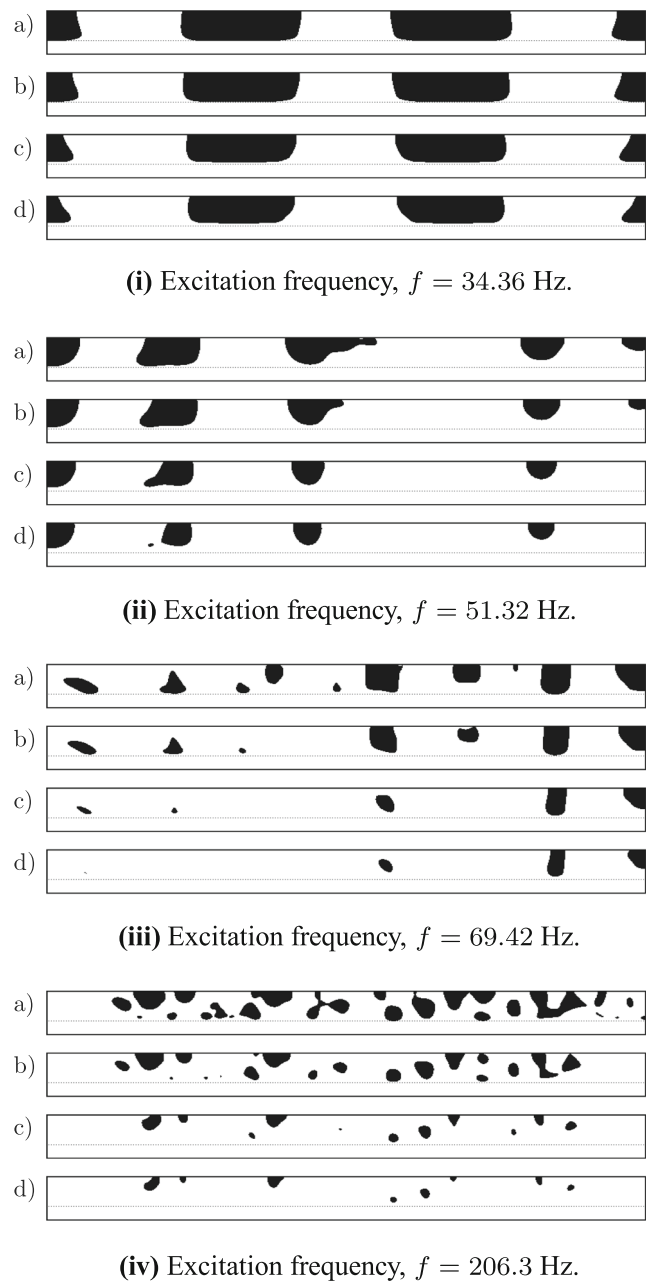


**Fig. 6** Projection of smoothed design variables for the four cases presented in Fig. 5i at different  $\eta$ -values: **a)**  $\eta = 0.3$ , **b)**  $\eta = 0.4$ , **c)**  $\eta = 0.6$ , **d)**  $\eta = 0.7$

### 10 Limiting the variations in $\tilde{\xi}$

This section presents two different methods for controlling the variation of the smoothed design variable field,  $\tilde{\xi}$  along with results of numerical experiments showing the benefits and limitations of the approaches. The first method is a new double filter approach. The second method, included for comparison, is a well known explicit penalization method (Bendsøe and Sigmund 2003) which here is applied to the filtered field,  $\xi$ , instead of the physical

design variables. Both methods allow the enforcement of a near 0/1  $\tilde{\xi}$ -field with intermediate values only near feature edges.

### 10.1 The double filter approach

The double filter approach consists of applying the density filter and projection introduced in Section 6 a second time on the already filtered and projected variables  $\tilde{\xi}(\mathbf{x})$ . In order to distinguish the two filter steps a subscript 1 and 2 are introduced to denote the first and second filter step respectively. The application of the double filter effectively solves the problem of the uncontrolled changes in the final smoothed design variables as will be demonstrated in the following.

The double filter approach introduces three additional parameters. These are a second filter radius  $R_2$ , a second projection strength  $\beta_2$  and a second projection level  $\eta_2$ . For all simulations done in the context of this paper, the parameters have been chosen to depend in a trivial manner on the parameters of the first filtering step effectively eliminating them. The second filter radius and projection strength have been chosen as  $R_2 = \frac{1}{2}R_1$  and  $\beta_2 = \frac{1}{2}\beta_1$  respectively. Regarding the projection level,  $\eta_2 = \eta_1$  has been chosen for the standard approach while for the robust approach it is no longer  $\eta_1$  that varies across realizations but instead  $\eta_2$ . For the robust approach the first projection level has been chosen as  $\eta_1 = \min_k \eta_{2,k}$ . These choices have worked well for all investigated cases.

Due to the  $\beta$ -continuation scheme the double filter works very similarly to the single filter in the beginning of the optimization process. This is because the projection for low values of  $\beta$  is close to inactive. Thus the second filter only further smooths the design variables without introducing other restrictions on the optimization. As  $\beta_1$  increases the first smoothing and projection step will produce a near 0/1 design. The second smoothing step then smooths the design along its edges while the second projection step controls the amount of material added/removed from each edge. For high  $\beta_2$ -values this gives control on how much the size of each feature in the design is changed as the projection level is varied. The amount of material removed in the projection step is controlled by  $\eta_2$  together with  $R_2$ . The relationship between  $\eta_2$  and the change in the size of the design features is analyzed for a 1D case in Schevenels et al. (2011). Here a lower bound is found which shows a nearly linear relationship for  $\eta_2 \in [0.3, 0.7]$ . Based on this analysis it is suggested to limit  $\eta_2$  to this, or a shorter, interval centered at 0.5 to ensure that for  $\beta_1 \gg 1$  all changes in the design will occur along its edges in a predictable near-uniform manner as the second projection level is varied. If features appear/disappear or agglomerate/separate as  $\eta_2$  is

varied they do so in a predictable fashion in contrast to what was observed with the single filter approach.

The choice of  $R_2$  relative to  $R_1$  is important. If  $R_2$  is chosen too large compared to  $R_1$  the functionality of the double filter is lost for the following reason. The first smoothing operation creates a functional dependence between design variables which are less than  $R_1$  apart. Thus the field  $\tilde{\xi}$  may in some sense be seen as a coarser version of the original design field. Filtering a second time with a large radius  $R_2$  can therefore be seen as functionally equivalent to smoothing only a single time on the unfiltered design variables. Thus unpredictable variations in the design with projection level may be observed if  $R_2$  is chosen to large. From our experimentation for the acoustic cavity problem it has been found that choosing  $R_2$  such that  $R_2 \leq \frac{R_1}{2}$  works well for all investigated cases. Choosing  $R_2 \geq R_1$  has been found to destroy the effect of the double filter in several cases.

The choice of  $\beta_2$  controls the sharpness of the second projection. Just as for the single filter, if  $\beta_2$  is chosen with a high initial value, it will force the optimizer to converge to a suboptimal local minimum since the design variable field is forced immediately towards 0/1.

The application of the double filter in 1D using high  $\beta$ -values in both projection steps is sketched in Fig. 7.

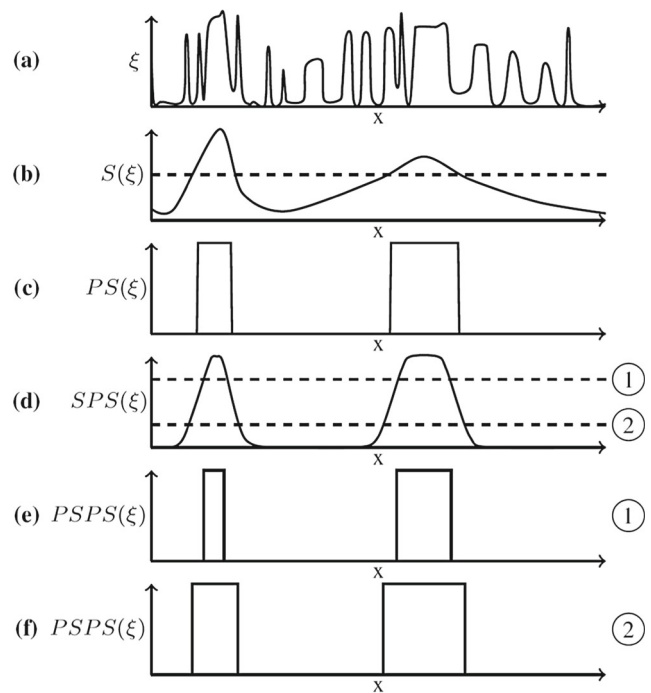


**Fig. 7** Sketch of the double filter applied to a function,  $\xi(x)$  in 1D (with  $\beta_1 \gg 1, \beta_2 \gg 1$ ). Two different projection levels are used for the second projection.  $S(\cdot)$  denotes smoothing and  $P(\cdot)$  denotes projection. **a**  $\xi(x)$ , **b**  $S_1(\xi(x))$ , **c**  $P_1(S_1(\xi(x)))$ , **d**  $S_2(P_1(S_1(\xi(x))))$ , **e**  $P_{2,1}(S_2(P_1(S_1(\xi(x)))))$ , **f**  $P_{2,2}(S_2(P_1(S_1(\xi(x)))))$



For  $\beta_1 \gg 1, \beta_2 \gg 1$  the sensitivity  $\frac{d\Phi}{d\xi_i}$  is zero unless  $\xi_i$  lie within the filter radius of the edge of a design feature. This effectively turns the optimization problem into a shape optimization problem at high  $\beta$ -values. Thus initially when the projection strength is low the design is free to form without any restrictions on its topology while in the final part of the optimization design features are only allowed to change shape or disappear. To ease the referencing of the design variables at different stages in the filtering process each stage will henceforth be denoted as S, PS, SPS and PSPS respectively. The S and P are short for, S: Smoothing, and P: Projecting. The ordering of the letters corresponds to the order of the application of the operators read from right to left.

A final note of importance is that the double filter approach does not guarantee a length scale in the design and therefore not a fixed topology across all projection levels. However in most practically considered cases a length scale was found to be present.

### 10.1.1 Sensitivities

Applying the density filter and projection on  $\tilde{\xi}$  is operationally identical to applying the same operations on  $\xi$ . Therefore the sensitivity modifications are straightforward<sup>2</sup>. The sensitivities for the double filter are given by,

$$\frac{d\Phi}{d\xi_i} = \sum_{h \in \mathcal{B}_{e,i}} \frac{\partial \tilde{\xi}_h}{\partial \xi_i} \frac{\partial \tilde{\xi}_h}{\partial \xi_h} \Delta \Phi_h, \quad i \in \{1, 2, \dots, N\}, \quad (28)$$

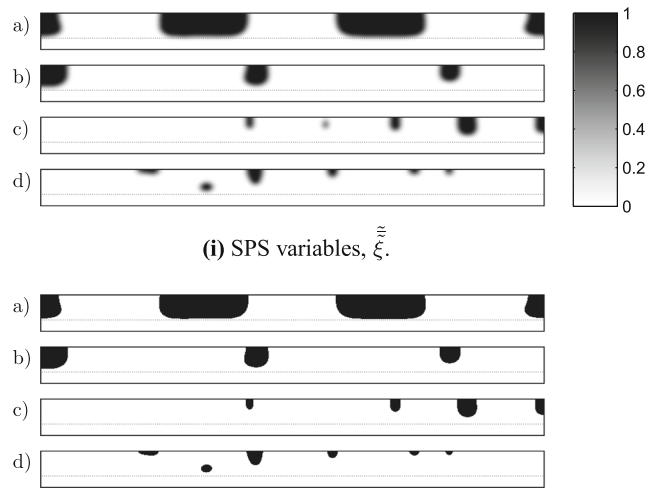
$$\Delta \Phi_h = \sum_{j \in \mathcal{B}_{e,h}} \frac{\partial \tilde{\xi}_j}{\partial \xi_h} \frac{\partial \tilde{\xi}_j}{\partial \xi_j} \frac{d\Phi}{d\xi_j}, \quad h \in \{1, 2, \dots, N\}. \quad (29)$$

While these expressions may look formidable, the computational requirements for calculating the sensitivities are only twice of those for the single filter which is very cheap compared to solving the FEM problem and the optimization problem.

### 10.2 Double filtered standard approach

The double filter has been used with the standard approach replacing the single filter. Results for the four excitation frequencies are presented here. The SPS variables and final designs (PSPS variables, projected at  $\eta_2 = 0.5$ ) are shown in Fig. 8i and ii, respectively.

Figure 8i clearly shows that the SPS-variables only change along design feature edges. Hence the problem of unpredictably varying intermediate design variable values



(ii) Final design (PSPS variables projection at  $\eta_2 = 0.5$ ).

**Fig. 8** (i) SPS and (ii) PSPS design variables for the four excitation frequencies, **a)**  $f = 34.36$  Hz, **b)**  $f = 51.32$  Hz, **c)**  $f = 69.42$  Hz, **d)**  $f = 206.3$  Hz. The standard approach with the double filter has been used for the optimization

has been resolved. Comparing the designs in Fig. 8ii to those in Fig. 3ii it is seen that for  $f \in \{69.42 \text{ Hz}, 206.3 \text{ Hz}\}$  both the topology and overall appearance of the designs have changed. These changes may be attributed to the additional restrictions on the optimization imposed by the double filter and the fact that many local minima exist for the model problems.

### 10.2.1 Sensitivity to design variations

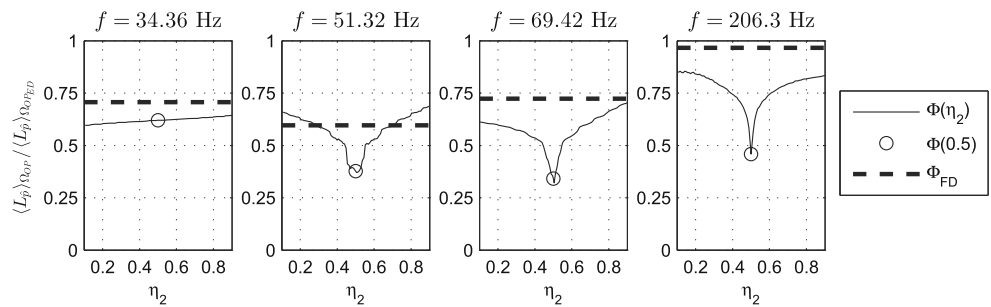
Using the double filter it is now meaningful to investigate the sensitivity of the designs towards near-uniform spatial variations by varying the projection level  $\eta_2$ . This has been done for  $\eta_2 \in [0.1, 0.9]$  which corresponds to a large near-uniform variation of approximately  $\pm 0.1$  meter ( $\approx \pm 4$  elements for the chosen discretization) for each design feature.  $\langle L \hat{p} \rangle_{\Omega_{OP}}(\eta_2)$  (scaled by  $\langle L \hat{p} \rangle_{\Omega_{OPED}}$ ) for each of the four excitation frequencies is shown in Fig. 9i. A dashed line showing  $\langle L \hat{p} \rangle_{\Omega_{OPFD}}$  (scaled by  $\langle L \hat{p} \rangle_{\Omega_{OPED}}$ ) corresponding to the average sound pressure level in  $\Omega_{OP}$  when simply filling the entire design domain with material has been included. The interested reader may use the value of  $\langle L \hat{p} \rangle_{\Omega_{OPED}}$  from Table 2 to obtain values in db SPL.

By considering  $\langle L \hat{p} \rangle_{\Omega_{OP}}(\eta_2 = 0.5)$  it can be seen that a significant reduction in SPL is obtained for all excitation frequencies for the nominal designs. A reduction between 40 and 70 percent is observed across the four frequencies. The design for  $f = 34.36$  Hz is observed to be highly robust with increases of only a few percent for large variations in projection level. For this low frequency the observed behavior is exactly what is expected since the wavelength is much

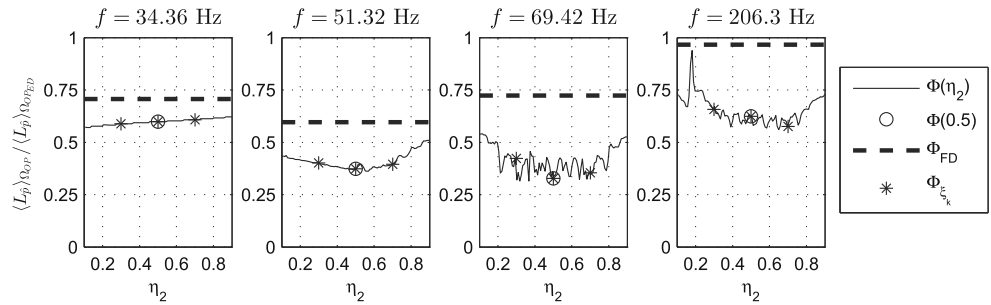
<sup>2</sup>The interested reader may find a derivation of the new sensitivities in Appendix.

**Fig. 9**  $\langle L_{\hat{p}} \rangle_{\Omega_{OP}} / \langle L_{\hat{p}} \rangle_{\Omega_{OP,ED}}$  as a function of projection level. **(i)** and **(ii)**:

$\langle L_{\hat{p}} \rangle_{\Omega_{OP}}(\eta_2) / \langle L_{\hat{p}} \rangle_{\Omega_{OP,ED}}$  is denoted by the thin black line. The performance of the nominal design ( $\eta_2 = 0.5$ ) is denoted by  $\circ$ . For comparison,  $\langle L_{\hat{p}} \rangle_{\Omega_{OP,ED}} / \langle L_{\hat{p}} \rangle_{\Omega_{OP,ED}}$  is denoted by a thick dashed black line. **(ii)**: The realisations of  $\eta_2$  for which the design has been optimized are denoted with  $*$



**(i)** Performance for designs presented in figure 8 obtained using the double filtered standard approach.



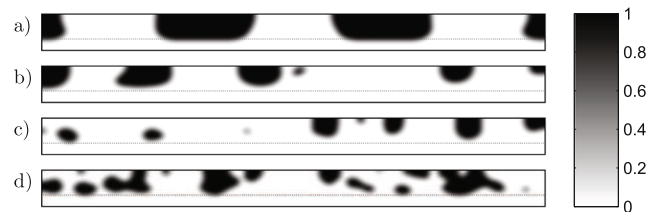
**(ii)** Performance for designs presented in figure 10 obtained using the double filtered robust approach.

longer than the design variations. Thus the variations are not expected to have much influence on the pressure-field. If one considers the three higher frequencies a different picture starts to emerge however. As a first example consider the case of  $f = 69.42$  Hz. Here an increase from  $\eta = 0.5$  to  $\eta = 0.55$  corresponding to a near-uniform decrease in feature size of approximately  $V_u \approx -1$  cm causes the relative performance improvement to deteriorate by more than 17 percent. As a second example consider the design optimized for  $f = 206.3$  Hz. Here a deterioration of  $\approx 24$  percent is observed for variations in  $\eta_2$  of about 0.05. Such large deteriorations in performance under small near-uniform variations are troublesome, especially considering that the scale is relative dB. What is observed from Fig. 8 is that the designs become increasingly sensitive towards small near-uniform geometric variations with increasing frequency. This high sensitivity towards spatial variations creates an interest in investigating a robust design approach.

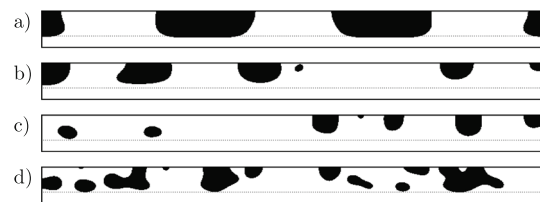
**10.3 Double filtered robust approach**

In order to investigate whether it is possible to obtain robust designs for all four excitation frequencies the robust approach with the double filter is used. The resulting SPS- and PSPS-variables for the nominal design are presented in Fig. 10. It is again observed that intermediate values of the SPS-variables are only found along the edges of design features. The design for  $f = 34.36$  Hz resembles the one optimized for a single projection level while the three

designs for the higher excitation frequencies are very different in both shape and topology. This agrees with the lack of robustness observed in Fig. 9i. Figure 11 shows projections of the SPS-variable at  $\eta_2 \in \{0.3, 0.4, 0.6, 0.7\}$ . From here it is clearly seen that PSPS-variables now vary in a spatially near-uniform manner with projection level.



**(i)** SPS-variables



**(ii)** Final design (PSPS second projection at  $\eta_2 = 0.5$ ).

**Fig. 10** **(i)** SPS and **(ii)** PSPS design variables for the four excitation frequencies, **a)**  $f = 34.36$  Hz, **b)**  $f = 51.32$  Hz, **c)**  $f = 69.42$  Hz, **d)**  $f = 206.3$  Hz. The designs has been obtained using the robust approach with the double filter using three realizations for the second projection,  $\eta_2 \in \{0.3, 0.5, 0.7\}$

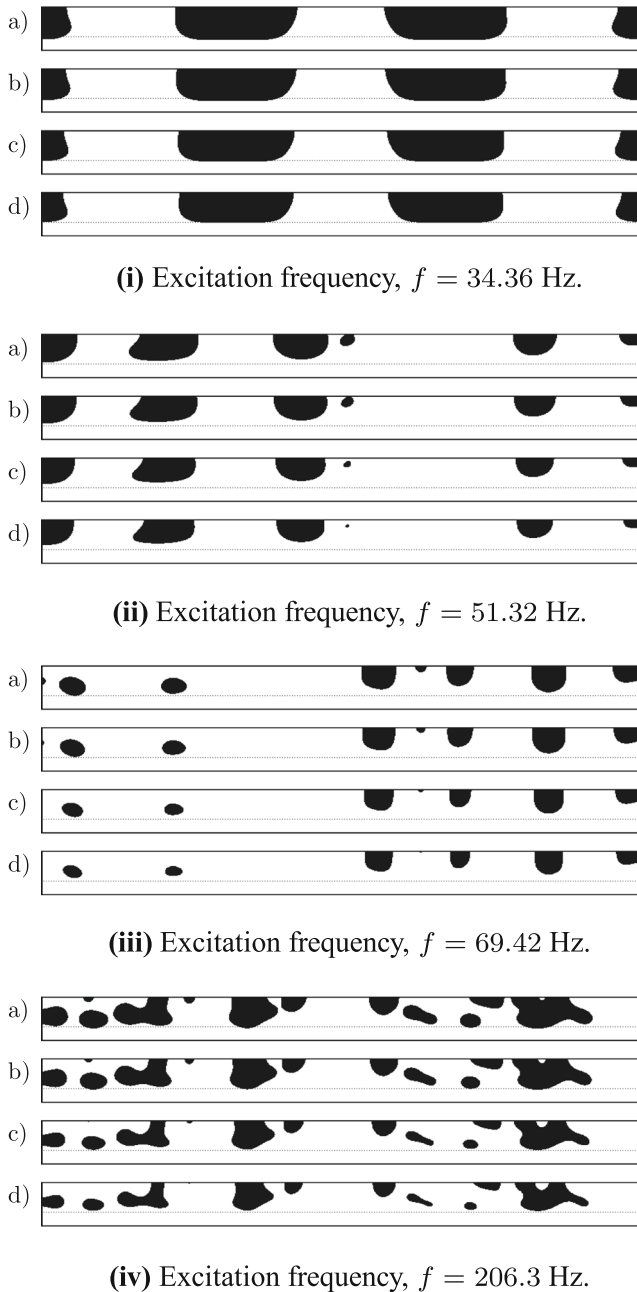


**Fig. 11** Projection of SPS design variables at four different  $\eta_2$ -values, **a)**  $\eta_2 = 0.3$ , **b)**  $\eta_2 = 0.4$ , **c)**  $\eta_2 = 0.6$ , **d)**  $\eta_2 = 0.7$  for the four designs shown in Fig. 10i

10.3.1 Sensitivity to design variations

Figure 9ii shows the variation in  $\langle L_{\hat{\rho}} \rangle_{\Omega_{OP}}(\eta_2) / \langle L_{\hat{\rho}} \rangle_{\Omega_{OPFD}}$  with  $\eta_2$  for the four designs presented in Fig. 10ii. All the designs are seen to perform robustly for large variations of  $\eta_2$  when compared to the results seen in Fig. 9i. For the case with  $f = 34.36$  Hz almost no change in performance is observed compared to Fig. 9i. For  $f = 51.32$  Hz the robustness of the performance is seen to have improved

for a large  $\eta_2$ -interval. Here the robust design maintain a performance improvement of 60 percent or more for  $\eta_2 \in [0.3, 0.7]$  compared to  $\langle L_{\hat{\rho}} \rangle_{\Omega_{OPFD}}$ . For  $f = 69.42$  Hz oscillations of up to 14 percent in performance improvement are observed. These are large fluctuations, however the performance increase for all  $\eta_2 \in [0.22, 0.78]$  is more than 55 percent, which compared to the performance observed in Fig. 9i is a significant improvement in robustness. For  $f = 206.3$  Hz oscillations of up to 10 percent are seen for  $\eta_2 \in [0.3, 0.7]$  however the performance improvement stays above 33 percent which is good compared to the non-robust case if perturbations of  $\eta_2$  of 0.05 or more is considered. Another important note is that the performance increase for the robust designs for the three lowest frequencies for all  $\eta_2 \in [0.3, 0.7]$  are very close to the level of the nominal design obtained using the standard approach. Thus optimizing the designs for robustness under near-uniform variations does not significantly reduce the obtained performance for the nominal designs.

10.4 The penalization approach

A well known way of restricting the number of  $\xi$ -variables taking intermediate values is to penalize the design field explicitly (Bendsøe and Sigmund 2003). The penalization can be done by either adding an artificial penalization term,  $\Phi_p$ , to the objective or introducing an additional constraint. Here we consider penalizing the filtered design variables,  $\tilde{\xi}$ , as suggested by Borrvall and Petersson (2001). The penalization term given in (30) is used.

$$\Phi_p(\mathbf{x}) = \alpha_{\Phi_p} \int \tilde{\xi}(\mathbf{x})(1 - \tilde{\xi}(\mathbf{x}))d\Omega_d / \int d\Omega_d, \quad \alpha_{\Phi_p} > 0. \tag{30}$$

The sensitivities of (30) with respect to  $\tilde{\xi}$  are trivial to calculate. The value of  $\Phi_p(\mathbf{x})$  is zero in areas with  $\tilde{\xi} = 0$  or  $\tilde{\xi} = 1$  while it assumes its maximum value for  $\tilde{\xi} = \frac{1}{2}$ . For sufficiently high values of  $\alpha_{\Phi_p}$  the approach forces the smoothed design variables towards 0/1 which will ensure narrow ranges of intermediate values for the smoothed design variables. This leads to near-uniform variations in the design along the edges of design features when the projection level is varied. While this attribute is appealing one significant problem exists: The choice of  $\alpha_{\Phi_p}$ . If  $\alpha_{\Phi_p}$  is chosen too large the penalization term will dominate the optimization which will result in poorly performing designs. If  $\alpha_{\Phi_p}$  is chosen too small, however, the penalization will not be effective and therefore the listed benefits are lost.

Designs obtained using the robust formulation where the penalization term has been added to the objective using  $\alpha_{\Phi_p} = 6 \cdot 10^{-2}$  are presented here. This choice of  $\alpha_{\Phi_p}$

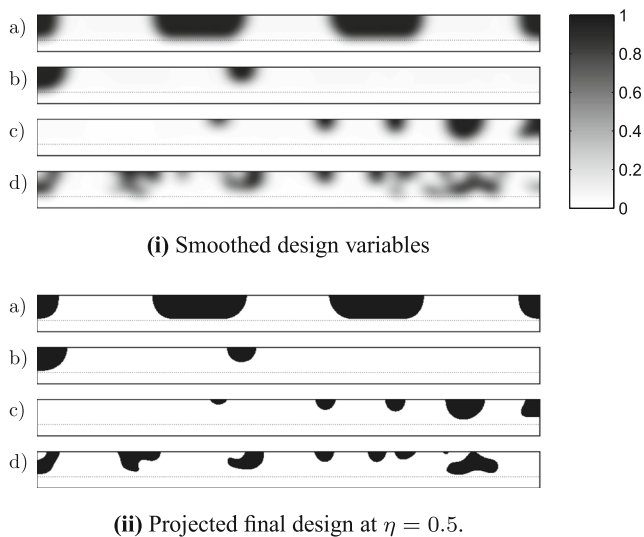


**Fig. 12** (i) Smoothed and (ii) projected design variables for the four excitation frequencies, **a**)  $f = 34.36$  Hz, **b**)  $f = 51.32$  Hz, **c**)  $f = 69.42$  Hz, **d**)  $f = 206.3$  Hz, obtained with the robust approach with three realizations and the penalisation term added to  $\Phi$  using  $\alpha_{\Phi_p} = 6 \cdot 10^{-2}$

illustrates both good and bad performance of the approach distributed over the four excitation frequencies. A filter range of  $R = 20$  has been used. The resulting designs are presented in Fig. 12.

From the figure it is seen that at the three lower excitation frequencies near  $0/1 \tilde{\xi}$  variables with smoothed edges along design features are obtained. Meanwhile for  $f = 206.3$  Hz this property is seen to have disappeared. Figure 13 shows the design obtained for  $f = 206.3$  Hz projected at the four different  $\eta$ -values. The design is seen to change topology and vary non-uniformly. Hence the design has not been optimized for near-uniform spatial variations as intended due to a too weak penalization. Another worrying result is the design obtained for the excitation frequency  $f = 51.32$  Hz. Here the choice of  $\alpha_{\Phi_p} = 6 \cdot 10^{-2}$  turns out to be too restrictive causing the optimization algorithm to get stuck in a local minimum with a poor performance. The performance obtained with this design is  $\langle L_{\hat{p}} \rangle_{\Omega_{op}} \approx 56$  dB for the

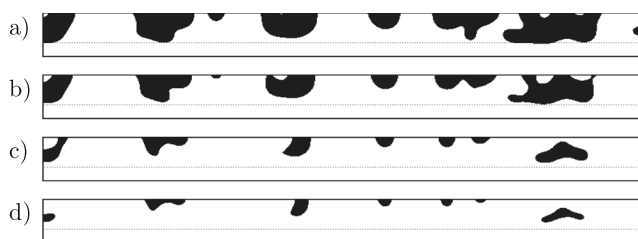


**Fig. 13** Smoothed design variables presented in Fig. 12i for the frequency,  $f = 206.3$  Hz projected at, **a**)  $\eta = 0.3$ , **b**)  $\eta = 0.4$ , **c**)  $\eta = 0.6$ , **d**)  $\eta = 0.7$

nominal design which is more than 19 dB worse than the performance of the design obtained using the double filter approach, as may be deduced from Fig. 9ii combined with  $\langle L_{\hat{p}} \rangle_{\Omega_{OPED}}$  from Table 2.

These examples illustrate the main problem with the penalization approach. That is, the correct choice of  $\alpha_{\Phi_p}$  depends on the parameters of the problem in a non-obvious way which makes experimentation necessary for each excitation frequency. On the other hand the examples also illustrate that if  $\alpha_{\Phi_p}$  is chosen correctly the approach may work well. For the excitation frequencies studied here results similar to those obtained using the double filter approach are obtained if  $\alpha_{\Phi_p}$  is chosen correctly.

## 11 Non-uniform design variations

We have demonstrated that using the robust approach with the double filter it is possible to create designs which are highly robust towards near-uniform geometric variations. In real applications however, during the production, installation and use of a given design it is more likely that small non-uniform errors are introduced. An interesting question now becomes whether small non-uniform variations (NUVs) cause significant deteriorations in performance for designs optimized for near-uniform variations. A natural extension of this question is to investigate whether it is possible to create designs that are more robust towards NUVs. In this section we demonstrate that by using the robust approach with the double filter it is possible to consider non-uniform variations in the optimization. We present results showing that the performance of designs optimized for near-uniform variations may deteriorate significantly under small NUVs. Then we show that it is possible to obtain designs that maintain a more robust performance under both non-uniform and near-uniform variations by including samples of the NUVs in the optimization process.

When taking NUVs into account during the optimization process a high number of realizations is needed in order to assure that the space of possible perturbations is covered. In this case the computational resources required for the standard FEM approach become a limiting factor. Therefore a hybrid finite element and wave based method (FE-WBM) was implemented, in order to reduce the cost of modeling the non-design domain, and used to obtain the results presented in the following. The wave based method was proposed by Desmet (1998) and the hybrid FE-WBM by Hal et al. (2003). The hybrid FE-WBM has just recently been applied to topology optimization by Goo et al. (2014). The strength of the hybrid method is that it is possible to significantly reduce the number of degrees of freedom used in the parts of the simulation domain where the model parameters are homogeneous.

The hybrid method is applied by discretizing the non-design domain  $\Omega_{\text{WBM}} = \Omega \setminus \Omega_d$  using a set of wave basis functions which are themselves solutions to the Helmholtz equation. This reduces the number of degrees of freedom needed in  $\Omega_{\text{WBM}}$  significantly. The design domain  $\Omega_d$  is still discretized exactly as described in Section 5. Finally the two domains are coupled by introducing a set of coupling degrees of freedom along the interface between the  $\Omega_{\text{WBM}}$  and  $\Omega_d$ . Since  $\Omega_d$  is discretized as described in Section 5 the parametrization of  $\xi(\mathbf{x})$ , the formulation of the optimization problem, the application of the smoothing and projection operators and the interpretation of the design domain does not change in any way.

By applying the hybrid method to the present problem where the ratio of the full model domain to the design domain is approximately  $\Omega_d \approx 0.1\Omega$  the computational time was reduced by approximately a factor of ten. We emphasize that other than a reduction in computational time the application of the hybrid FE-WBM method does not change the optimization problem in any way and as such all results may be replicated using pure FEM if sufficient computational resources are available. The reported performance of all the designs obtained using the hybrid method was acquired using a pure FEM discretization.

A slightly different model problem, illustrated in Fig. 14, was considered in the following. Here the vibrational source was moved to one of the outer domain boundaries and was imposed using (3) keeping  $U = 0.01$ , hence modeling a vibrating piston set in the wall. The movement of the source was done solely due to implementation choices made for the WBM-FEM hybrid method which required placing the source on the domain boundary.

It is possible to model NUVs in many ways. One way is to consider random non-uniform variations as was done for structural and heat conduction problems by Schevenels et al. (2011) and Lazarov et al. (2012). In the present

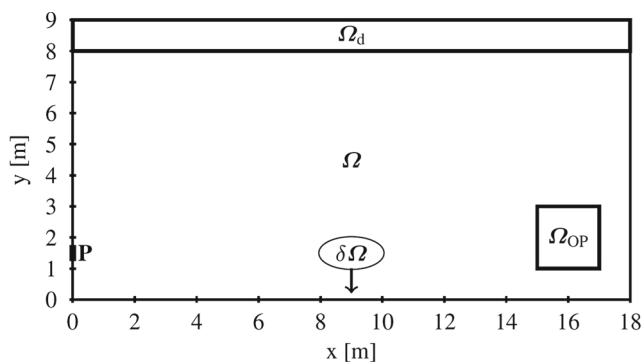


**Fig. 14** Illustration of the modified model problem domain.  $\Omega_{\text{OP}} \in [15.5, 16.5] \times [1.5, 2.5]$  is the optimization domain,  $\Omega_d \in [0, 18] \times [8, 9]$  is the design domain and  $\mathbf{P} \in 0 \times [1.3, 1.7]$  denotes the region where an acoustic excitation is imposed

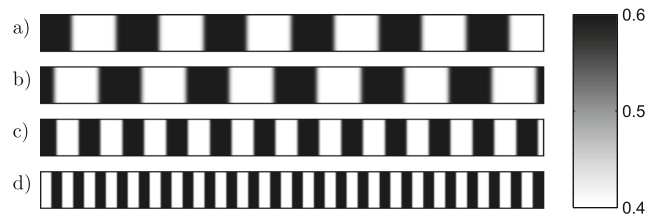


**Fig. 15** Samples of the non-uniformly varying projection field for **a)**  $B = 2, C = \frac{4}{5}\pi$ , **b)**  $B = 2, C = \frac{6}{5}\pi$ , **c)**  $B = 4, C = \frac{6}{5}\pi$ , **d)**  $B = 8, C = \frac{8}{5}\pi$

case we consider only one type of non-random variation. Namely sinusoidal variations in one spatial direction and no variation in the other. This is only a small subset of all possible NUVs but it works for illustrating the desired points. The NUVs are included in the optimization process by introducing a variable projection field,  $\eta(\mathbf{x})$ , (Schevenels et al. 2011). This field replaces the constant projection level  $\eta$ , leading to varying projection levels across the domain. When using the double filter approach it is  $\eta_2$  which is replaced with the varying projection field. The NUVs in the projection level have been modeled as,

$$\eta_2(\mathbf{x}) = \eta_{\min} + (\eta_{\max} - \eta_{\min}) \cdot P(A \cdot \cos(Bx + C)). \quad (31)$$

Here  $P$  is the normal cumulative distribution function with unit standard deviation and unit mean.  $\eta_{\max} \in ]\eta_{\min}, 1]$  and  $\eta_{\min} \in [0, \eta_{\max}[$  are the maximum and minimum projection values, respectively.  $B$  and  $C$  were allowed to vary while  $A$  was kept fixed. Samples of the projection field for different  $B$  and  $C$  are shown in Fig. 15.

For the results presented here the following values have been used for the non-uniformly varying projection field:  $A = 6, B \in \{2, 4, 8\}, C \in [0, 2\pi], \eta_{\min} = 0.4$  and  $\eta_{\max} = 0.6$ . The optimizations were initialized with the material fraction  $\xi_{\text{ini}} = 0.5 \forall \mathbf{x} \in \Omega_d$  and a filter radius of  $R = 16$  was used.

### 11.1 Imposing NUV on robust designs

In the following the two excitation frequencies,  $f \in \{69.42, 206.3\}$  Hz are considered. Optimized designs were created using the robust approach with the double filter and three realizations of the second projection at  $\eta_2 \in \{0.3, 0.5, 0.7\}$ . The designs are presented in Fig. 16.

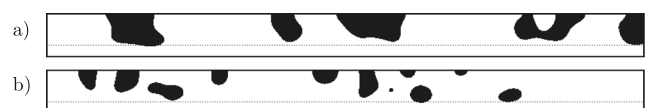


**Fig. 16** Nominal designs optimized using uniform variations for the excitations frequencies **a)**  $f = 69.42$  Hz, and **b)**  $f = 206.3$  Hz

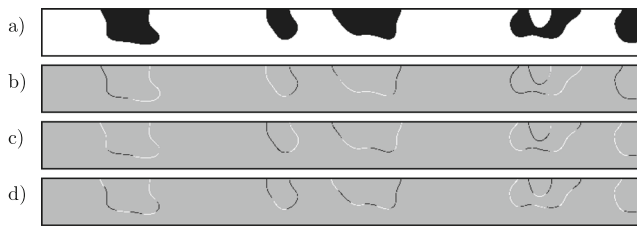


**Fig. 17** Non-uniform variations in the design optimized for  $f = 69.42$  Hz. **a)** Design. **b)-d)** Difference between the nominal design and the non-uniformly perturbed designs. White shows removed material and black shows added material

The designs were subjected to small non-uniform variations given by (31). Figure 17 shows representative examples of the non-uniform changes in the design optimized for  $f = 69.42$  Hz when the variations are imposed. In the sub figures **b)-d)** the white areas denote removed material while the black areas denote added material.

It is seen that the non-uniform variations are small (2.5 cm - 5 cm in terms of the model dimensions). Nevertheless a significant reduction in performance is observed. Figure 18 shows  $\langle L\hat{\rho} \rangle_{\Omega_{OP}}(\eta_2) / \langle L\hat{\rho} \rangle_{\Omega_{OP,ED}}$  for varying projection level,  $\eta \in [0.3, 0.7]$  overlaid with a graph of  $\langle L\hat{\rho} \rangle_{\Omega_{OP}}(\eta_{2,k}(\mathbf{x})) / \langle L\hat{\rho} \rangle_{\Omega_{OP,ED}}$  for 80 different realizations of the non-uniform variations with  $A = 6$ ,  $B \in \{2, 4, 8, 16\}$  and  $C$  uniformly distributed at 20 points in  $[0, 2\pi[$ .

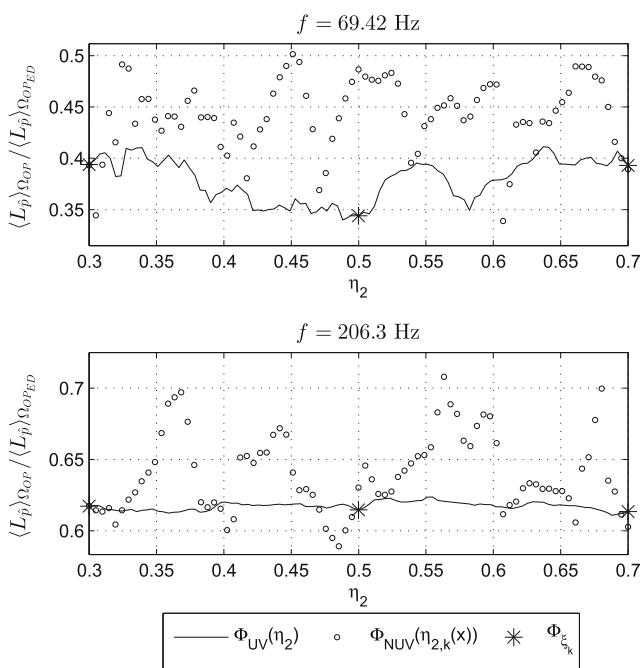


**Fig. 18**  $\langle L\hat{\rho} \rangle_{\Omega_{OP}} / \langle L\hat{\rho} \rangle_{\Omega_{OP,ED}}$  for designs in Fig. 16 exposed to near-uniform,  $\Phi_{UV}(\eta_2)$ , and non-uniform,  $\Phi_{NUV}(\eta_{2,k}(\mathbf{x}))$ , spatial variations. The performance at the three realization for which the designs were optimized,  $\Phi_{\epsilon_k}$ , are marked

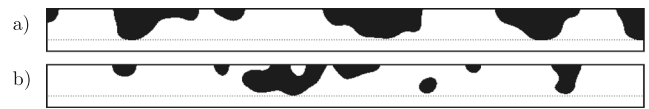


**Fig. 19** Nominal designs optimized using non-uniform variations for **a)**  $f = 69.42$  Hz, and **b)**  $f = 206.3$  Hz

Figure 18 clearly shows the lack of robustness of the designs towards non-uniform variations. The observed performance deteriorations are less significant than what was seen by comparing designs optimized using the robust approach and using the standard approach under near-uniform variations, however they are clearly still significant. Compared to the nominal designs ( $\eta_2 = 0.5$ ) a deterioration of up to 15 % is seen for the design optimized at  $f = 69.42$  Hz and up to 9 % for the design optimized at  $f = 206.3$  Hz. Considering comparable near-uniform variations ( $\eta_2 \in [0.4, 0.6]$ ) we only observe deteriorations of 5 % and 1 % respectively.

### 11.2 Optimizing for NUV

In order to reduce the observed deterioration in performance under non-uniform variations a new optimization was performed using the robust approach with the double filter. Here non-uniform variations were included in the realizations. A total of 18 realizations were used. Three used the constant projection levels  $\eta_2 \in \{0.3, 0.5, 0.7\}$ . The remaining fifteen realizations used the variable projection level

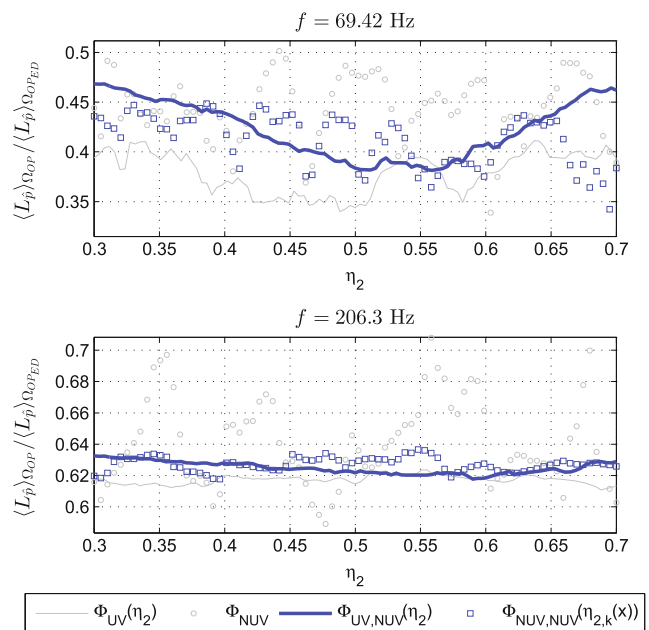
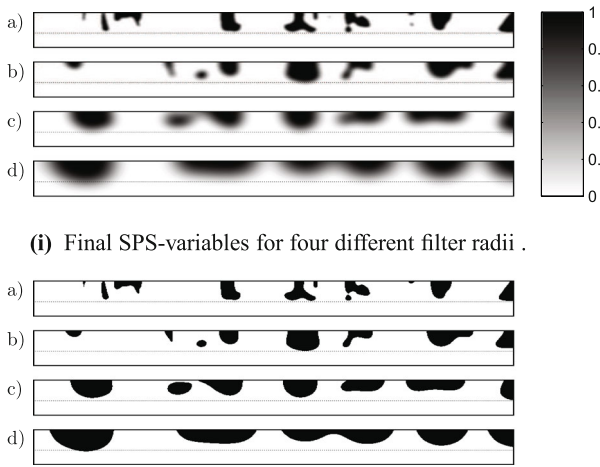
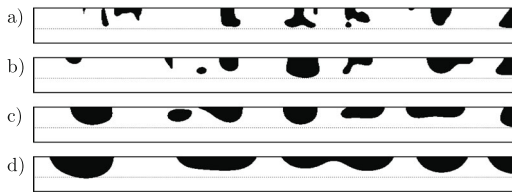


**Fig. 20**  $\langle L\hat{\rho} \rangle_{\Omega_{OP}} / \langle L\hat{\rho} \rangle_{\Omega_{OP,ED}}$  for the designs in Fig. 19 exposed to near-uniform,  $\Phi_{UV,NUV}(\eta_2)$ , and non-uniform,  $\Phi_{NUV,NUV}(\eta_{2,k}(\mathbf{x}))$ , variations. For easy comparison the data from Fig. 18 is plotted in light gray



(i) Final SPS-variables for four different filter radii .



(ii) Final PPS-variables for four different filter radii projected at  $\eta_2 = 0.5$ .

**Fig. 21** (i) SPS and (ii) PPS design variables obtained using the robust approach with different filter radii and six realizations of the uniform projection level at  $\eta_{2,k} \in \{0.3, 0.38, 0.46, 0.54, 0.62, 0.7\}$  for the excitation frequency  $f = 69.42$  Hz, discretized using  $(n_x, n_y) = (720, 360)$  finite elements. SPS-variables (i). a)  $R_1 = 10$  (i). b)  $R_1 = 20$  (i). c)  $R_1 = 40$  (i). d)  $R_1 = 60$ . (ii) PPS-variables projected at  $\eta_2 = 0.5$  for designs in (i)

given by (31) with all combinations of  $B \in \{2, 4, 8\}$  and  $C \in \left\{ \frac{2}{5}\pi, \frac{4}{5}\pi, \frac{6}{5}\pi, \frac{8}{5}\pi, 2\pi \right\}$ . Figure 19 show the designs resulting from the optimizations.

The performance of the designs under both near-uniform and non-uniform variations have been investigated in the same manner as in the previous section. The results are presented in Fig. 20.

From Fig. 20 it is immediately observed that the designs optimized for the non-uniform variations are more robust under non-uniform variations than the designs only optimized for uniform variations. Considering first the design for  $f = 69.42$  Hz. Here the ratio of  $\langle L_{\hat{\rho}} \rangle_{\Omega_{OP}} / \langle L_{\hat{\rho}} \rangle_{\Omega_{OPED}}$  for all variations in  $\eta_2$  within  $[0.4, 0.6]$  is now under 45 %

compared to the earlier design’s 50 %. Thus an improvement in worst case performance of 5 %. The trade off is a decrease in performance of the nominal design by approximately 4 % compared to the earlier design. Consider now the design optimized for  $f = 206.3$  Hz. This design is seen to perform highly robustly under both near-uniform and non-uniform variations with a maximum of 2 % variation in performance. The deterioration in performance of the nominal design compared to the earlier design is only 1 % while the worst case performance is now below 64 % compared to the earlier 71 %. Hence a 7 % better worst case performance.

A thorough study of the performance of the designs in Fig. 19 with more than 2500 realizations for uniformly distributed value of  $B \in [2, \dots, 16]$  and  $C \in [0, 2\pi]$  was performed to assure the correctness of the conclusions drawn above. This test did not reveal any results that contradict our conclusions for the presented cases.

### 12 Varying the filter radius

This section investigates the behavior of the double filter approach for varying filter radius. We consider the model problem in Fig. 14 and take the excitation frequency to be,  $f = 69.42$  Hz. We optimize using the doubly filtered robust approach for four different filter radii  $R_1 \in \{10, 20, 40, 60\}$  elements,  $R_2 = \frac{1}{2}R_1$  and near-uniform variations. We use six realizations for the projection level,  $\eta_{2,k} \in \{0.3, 0.38, 0.46, 0.54, 0.62, 0.7\}$ . The remaining parameters are set at the values given in Table 1. The reason for using six realizations for  $\eta_{2,k}$  instead of three as in the earlier cases is that it we found that for  $R_1 \in \{40, 60\}$  three realization for the second projection level are not enough to obtain a high performance across all values of  $\eta_2 \in [0.3, 0.7]$ . This finding is sensible since increasing  $R_1$  while keeping the variation in  $\eta_2$  fixed leads to an increased spatial variation in the design. Figure 21 presents

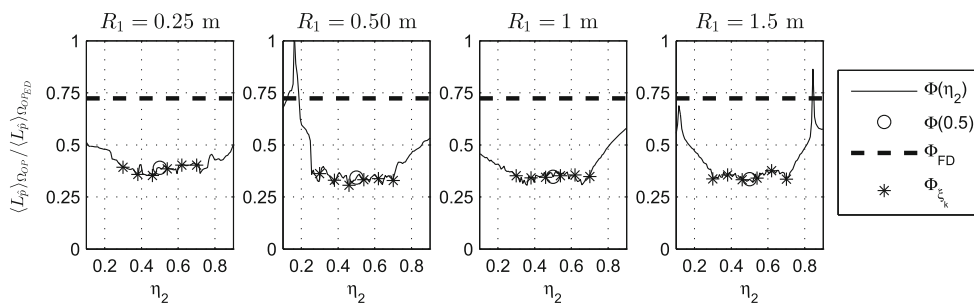


**Fig. 22**  $\langle L_{\hat{\rho}} \rangle_{\Omega_{OP}} / \langle L_{\hat{\rho}} \rangle_{\Omega_{OPED}}$  as a function of projection level for designs presented in Fig. 21, obtained using the double filtered robust approach, under uniform erosion/dilation.  $\langle L_{\hat{\rho}} \rangle_{\Omega_{OP}}(\eta_2) / \langle L_{\hat{\rho}} \rangle_{\Omega_{OPED}}$  is denoted by the thin black line. The performance of the nominal design

( $\eta_2 = 0.5$ ) is denoted by  $\circ$ . For comparison,  $\langle L_{\hat{\rho}} \rangle_{\Omega_{OPED}} / \langle L_{\hat{\rho}} \rangle_{\Omega_{OPED}}$  is denoted by a thick dashed black line. The realizations of  $\eta_2$  for which the design has been optimized are denoted with \*

the final SPS- and SPSP-variables for the four different cases.

It is seen that the double filter performs as expected for all filter radii, in the sense that it produces SPS-variables which consists of areas of material ( $\tilde{\xi}(\mathbf{x}) = 1$ ) with smoothed edges. Figure 22 shows the performance of each of the four designs under near-uniform erosion/dilation performed by varying  $\eta_2$  in the interval  $[0.1, 0.9]$ .

It is observed that the performance is similar in terms of the reduction in dB SPL for all four cases inside the interval of optimization.

### 13 Conclusions

We considered the minimization of sound pressure in part of a 2D domain for an acoustic cavity problem by placing material in another part of the domain using topology optimization. We showed that the direct application of a standard technique for robust topology optimization encounters a problem of uncontrollable intermediate design variables making it unusable. A novel double filter was introduced and it was shown to alleviate the problem thus allowing for the application of the robust optimization approach. It was demonstrated that small near-uniform geometric variations can cause significant deteriorations in the performance of designs optimized using the standard approach. Applying the robust approach with the double filter and optimizing for near-uniform geometric variations was shown to create highly robust designs under large near-uniform variations for all investigated frequencies. It was then demonstrated that imposing small non-uniform variations on designs optimized for near-uniform variations could lead to smaller but still significant deteriorations in performance. Finally it was shown to be possible to obtain designs which performed robustly under both near-uniform and selected non-uniform geometric variations by taking both types of variations into account during the optimization process. The proposed double filter approach is useful for highly shape sensitive optimization problems as demonstrated here. For less sensitive problems standard single filter approaches may be sufficient. When solving the acoustic cavity problem considered in this paper for a wider frequency band instead of for a single frequency (or narrow frequency band) the extreme sensitivity disappears and the problem may be solved using the single filter approach, see [Appendix](#).

**Acknowledgments** This work was financially supported by Villum Fonden through the research project *Topology Optimization - the Next Generation NextTop*.

## Appendix

### Derivation of sensitivities for the double filter

The sensitivities,  $\frac{d\Phi}{d\xi_i}$ , for the double filter may be derived as follows:

1. Apply the chain rule for calculating the sensitivities.

$$\frac{d\Phi}{d\xi_i} = \sum_{j,k,l,h} \frac{\partial \tilde{\xi}_l}{\partial \xi_i} \frac{\partial \tilde{\xi}_h}{\partial \tilde{\xi}_l} \frac{\partial \tilde{\xi}_k}{\partial \tilde{\xi}_h} \frac{\partial \tilde{\xi}_j}{\partial \tilde{\xi}_k} \frac{d\Phi}{d\tilde{\xi}_j}. \quad (32)$$

2. Eliminate two sums using the fact that  $\frac{\partial \tilde{\xi}_h}{\partial \tilde{\xi}_l} = 0 \forall l \neq h$  and that  $\frac{\partial \tilde{\xi}_j}{\partial \tilde{\xi}_k} = 0 \forall k \neq j$  due to the locality of (23).

$$\frac{d\Phi}{d\xi_i} = \sum_j \sum_h \frac{\partial \tilde{\xi}_h}{\partial \xi_i} \frac{\partial \tilde{\xi}_h}{\partial \tilde{\xi}_j} \frac{\partial \tilde{\xi}_j}{\partial \tilde{\xi}_j} \frac{d\Phi}{d\tilde{\xi}_j} \quad i \in \{1, 2, \dots, N\}. \quad (33)$$

3. Utilize that  $\tilde{\xi}_h$  only depends on the design variables  $\xi_i$  within the density filter radius reducing the sum over  $h$  significantly. The same argument applied to  $\tilde{\xi}_j$  and  $\tilde{\xi}_h$  reduces the sum over  $j$ . The set of indices for the dependent variables are denoted,  $\mathcal{B}_{e,i}$  and  $\mathcal{B}_{e,h}$  respectively. The sensitivities now take the form,

$$\frac{d\Phi}{d\xi_i} = \sum_{j \in \mathcal{B}_{e,h}} \sum_{h \in \mathcal{B}_{e,i}} \frac{\partial \tilde{\xi}_h}{\partial \xi_i} \frac{\partial \tilde{\xi}_h}{\partial \tilde{\xi}_j} \frac{\partial \tilde{\xi}_j}{\partial \tilde{\xi}_j} \frac{d\Phi}{d\tilde{\xi}_j}. \quad (34)$$

4. Rewriting the expression gives,

$$\frac{d\Phi}{d\xi_i} = \sum_{h \in \mathcal{B}_{e,i}} \frac{\partial \tilde{\xi}_h}{\partial \xi_i} \frac{\partial \tilde{\xi}_h}{\partial \tilde{\xi}_h} \left[ \sum_{j \in \mathcal{B}_{e,h}} \frac{\partial \tilde{\xi}_j}{\partial \tilde{\xi}_h} \frac{\partial \tilde{\xi}_j}{\partial \tilde{\xi}_j} \frac{d\Phi}{d\tilde{\xi}_j} \right]. \quad (35)$$

5. For a given  $h$  the expression in the bracket in (35) only depends on  $j$ . Thus we may define,

$$\Delta\Phi_h = \sum_{j \in \mathcal{B}_{e,h}} \frac{\partial \tilde{\xi}_j}{\partial \tilde{\xi}_h} \frac{\partial \tilde{\xi}_j}{\partial \tilde{\xi}_j} \frac{d\Phi}{d\tilde{\xi}_j}, \quad h \in \{1, 2, \dots, N\}. \quad (36)$$

This illustrates that the application of the double filter simply corresponds to applying the single filter twice.  $\square$

### Application of robust approach for frequency bands

Single frequency problems have been the focus of the paper due to the high sensitivity in the performance of the



optimized designs under geometric variations. In this section we provide an example showing the method applied for a band of frequencies as well. As will be demonstrated, this problem is far less sensitive towards geometric variations in the design. A requirement for considering optimization for a band of frequencies for the cavity problem is that a small amount of damping is added to the model problem to avoid problems caused by resonances in the frequency band of interest. The need for damping has nothing to do with the double filter or the robust approach and must be added regardless of the optimization strategy. Mass proportional damping is introduced by adding the term “ $\alpha_{\text{damp}} i \hat{\omega} \hat{p}$ ” to (7) where  $\alpha_{\text{damp}} = 0.01$  is the damping factor.

In the following we consider the model problem presented in Fig. 14 and seek to minimize the mean of the average sound pressure in  $\Omega_{\text{OP}}$  over a 1/3 octave frequency band,  $f_b \approx [61.85, 77.92]$  Hz, centered at,  $f_c = 62.5$  Hz. The objective function may thus be stated as,

$$\Phi(\xi) = \frac{1}{N_i} \sum_{i=1}^{N_i} \frac{1}{A_{\text{OP}}} \int |\hat{p}(\xi, f_i)|^2 d\Omega_{\text{OP}}, \tag{37}$$

where  $f_i$  are the frequencies optimized for and  $N_i$  is the number of frequencies. An optimization is performed using the standard approach with the double filter and the second projection at  $\eta_2 = 0.5$ . For comparison an optimization is performed using the robust approach with double filtering and five realizations of the second projection level,  $\eta_2 \in \{0.3, 0.4, 0.5, 0.6, 0.7\}$ . For both cases we use  $N_i = 20$  and consider equidistant frequencies in  $f_b$  including both endpoints. For the PDE problem we use a pure FEM discretization with  $\mathcal{N}_x = 216$ ,  $\mathcal{N}_y = 108$  elements. A filter range of  $R_1 = 5$  elements is used. Figure 23 shows the resulting SPS and SPSP variables for the two optimizations.

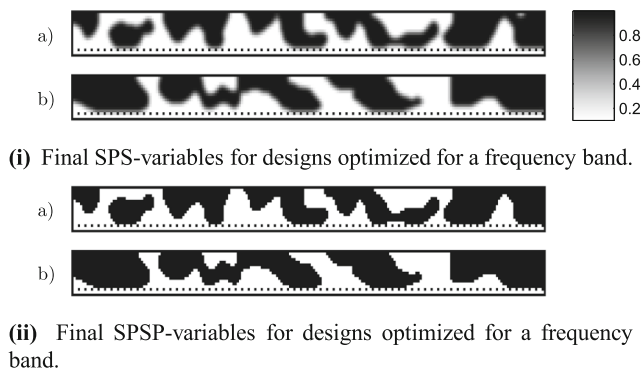


**Fig. 23** (i) SPS and (ii) SPSP design variables obtained using the a) standard and b) robust approach for the 1/3 octave frequency band optimization

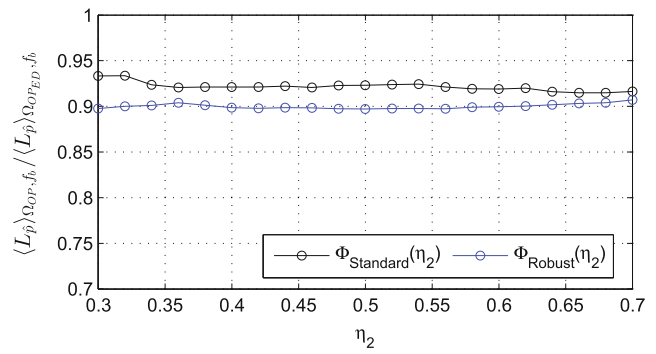


**Fig. 24**  $\langle L_{\hat{p}} \rangle_{\Omega_{\text{OP}}, f_b} / \langle L_{\hat{p}} \rangle_{\Omega_{\text{OPED}}, f_b}$  for the designs in Fig. 23 under near-uniform variations imposed by varying  $\eta_2$ . The performance of the designs is seen to be almost constant under the prescribed uniform variations

Figure 24 shows the mean of the average sound pressure level in  $\Omega_{\text{OP}}$  over the 1/3 octave frequency band,  $\langle L_{\hat{p}} \rangle_{\Omega_{\text{OP}}, f_b}$ , scaled by the same quantity in  $\Omega_{\text{OP}}$  for the empty cavity,  $\langle L_{\hat{p}} \rangle_{\Omega_{\text{OPED}}, f_b} \approx 89.79$  dB, as a function of projection level  $\eta_2$ , for both the standard and the robust approach. The mean over the frequency is calculated using 100 equidistant frequencies in  $f_b$ . This variation in projection level corresponds to a near-uniform erosion/dilation of 1 element or approximately 8 cm in the design. The presented results have been evaluated with the same amount of damping as the one used in the optimization.

From the figure it is clearly observed that both the standard and robust approach produce results which do not show any significant sensitivity towards uniform erosion or dilation of the design. It is noted that the robust approach produces a design with better performance. This is likely due to the additional restrictions on the optimization when using the robust approach which eliminates the local minimum trapping the optimization performed with the standard approach.

An investigation of the sensitivity of the performance under non-uniform geometric variations for the design optimized using the standard approach is also performed. Here it is shown that, just as for the uniform geometric perturbations, the sensitivity drops significantly when considering a band of frequencies compared to a single frequency. Twenty five non-uniform geometric variations are applied as described in Section 11 using  $A = 6$ ,  $B \in \{2, 3.5, 5, 6.5, 8\}$ ,  $C \in 2\pi \cdot \{1, 2, 3, 4, 5\}$ ,  $\eta_{\text{min}} = 0.3$ ,  $\eta_{\text{max}} = 0.7$ . Figure 25i show the sensitivity of the performance under the twenty five non-uniform geometric variations for the average response over  $f_b$  while Fig. 25ii show the performance sensitivity under the same twenty five non-uniform geometric variations for the single frequency  $f_s = 70.15$  Hz.

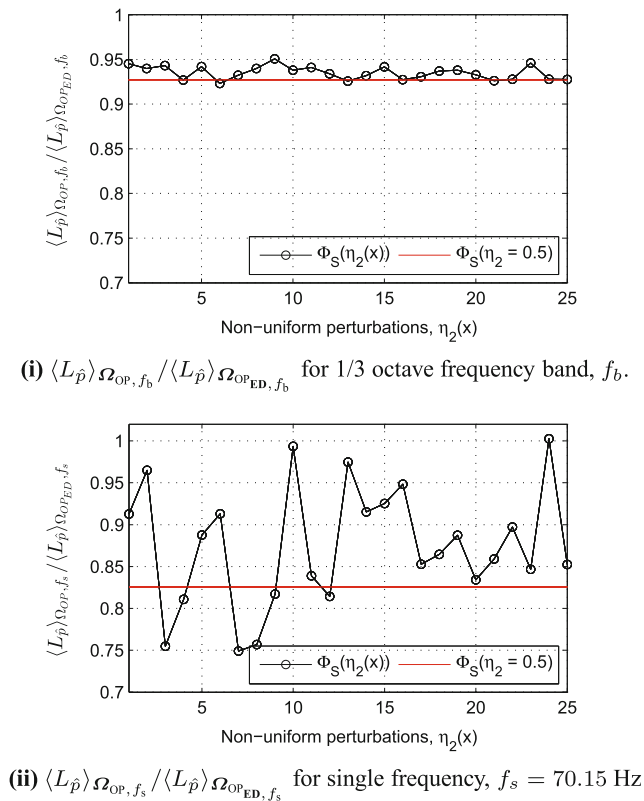


**Fig. 25** Scaled performance for the design in Fig. 23. a) under non-uniform variations imposed through  $\eta_2(x)$ . The performance of the design is seen to be less sensitive for a frequency band (i) than for a single frequency (ii). The red line marks the performance of the nominal design while the black line with circles mark the performance for the perturbed design

From the figure it is clearly seen that the average response over  $f_b$  is far less sensitive to geometric perturbations than when only considering  $f_s$ .

## References

- Bendsøe MP, Sigmund O (2003) Topology optimization - theory, methods and application. Springer
- Borrvall T, Petersson J (2001) Topology optimization using regularized intermediate density control. Computer methods in applied mechanical and engineering 190:4911–4928
- Bourdin B (2001) Filters in topology optimization. Int J Numer Methods Eng 50:2143–2158
- Bruns TE, Tortorelli DA (2001) Topology optimization of nonlinear elastic structures and compliant mechanisms. Computational Methods for Applied Mechanical Engineering 190:3443–3459
- Clausen A, Aage N, Sigmund O (2015) Topology optimization of coated structures and material interface problems. Computational Methods for Applied Mechanical Engineering 290:524–541
- Desmet W (1998) A wave based prediction technique for coupled vibro-acoustic analysis. PhD thesis, Katholieke Universitet Leuven
- Dürring MB, Jensen JS, Sigmund O (2008) Acoustic design by topology optimization. J Sound Vib 317:557–575
- Du J, Olhoff N (2007) Minimization of sound radiation from vibrating bi-material structures using topology optimization. Structural and Multidisciplinary Optimization 33:305–321
- Elesin Y, Lazarov B, Jensen J, Sigmund O (2012) Design of robust and efficient photonic switches using topology optimization. Photonics and Nanostructures Fundamentals and Applications 10: 153–165
- Goo S, Kook J, Koo K, Hyun J, Wang S (2014) Acoustic topology optimization for interior acoustic problem using the hybrid finite element - wave based method. In: The Eighth China-Japan-Korea Joint Symposium on Optimization of Structural and Mechanical Systems
- Guest JK, Prévost JH, Belytschko T (2004) Achieving minimum length scale in topology optimization using nodal design variables and projection functions. Int J Numer Methods Eng 61:238–254
- Hal BV, Desmet W, Pluymers B, Sas P, Vandepitte D (2003) A coupled finite element - wave based approach for the steady-state dynamics analysis of acoustic systems. J Comput Acoust:285–303
- Jacobsen F, Juhl PM (2013) Fundamentals of General Linear Acoustics. Wiley
- Kook J, Koo K, Hyun J, Jensen JS, Wang S (2012) Acoustical topology optimization for zwicker's loudness model - application to noise barriers. Computational Methods for Applied Mechanical Engineering 237:130–151
- Lazarov BS, Schevenels M, Sigmund O (2012) Topology optimization considering material and geometric uncertainties using stochastic collocation methods. Structural Multidisciplinary Optimization 46:597–612
- Lee JW, Kim YY (2009) Rigid body modeling issue in acoustic topology optimization. Computational Methods for Applied Mechanical Engineering 198:1017–1030
- Lyon RH, DeJONG RG (1998) Statistical Energy Analysis. RH Lyon Corp
- Schevenels M, Lazarov B, Sigmund O (2011) Robust topology optimization accounting for spatially varying manufacturing errors. Computational Methods for Applied Mechanical Engineering 200:3613–3627
- Sigmund O (2009) Manufacturing tolerant topology optimization. Acta Mech Sinica 25:227–239
- Svanberg K (1987) The method of moving asymptotes - a new method for structural optimization. Int J Numer Methods Eng 24:359–373
- Wadbro E (2014) Analysis and design of acoustic transition sections for impedance matching and mode conversion. Structural and Multidisciplinary Optimization 50:395–408
- Wadbro E, Berggren M (2006) Topology optimization of an acoustic horn. Computational Methods for Applied Mechanical Engineering 196:420–436
- Wang F, Jensen JS, Sigmund O (2011a) Robust topology optimization of photonic crystal waveguides with tailored dispersion properties. Opt Soc Am 28:387–397
- Wang F, Lazarov BS, Sigmund O (2011b) On projection methods, convergence and robust formulations in topology optimization. Structural Multidisciplinary Optimization 43:767–784
- Xu S, Cai Y, Cheng G (2010) Volume preserving nonlinear density filter based on heaviside projections. Structural and Multidisciplinary Optimization 41:495–505
- Yoon GH, Jensen JS, Sigmund O (2007) Topology optimization of acoustic-structure interaction problems using a mixed finite element formulation. Int J Numer Methods Eng 70:1049–1075